Data-driven analysis of interactions between pairs and ensembles of coupled dynamics

Petroula Laiou

TESI DOCTORAL UPF / ANY 2017

DIRECTOR DE LA TESI
Prof. Dr. Ralph Gregor Andrzejak Departament DTIC

Acknowledgments

When I started writing my thesis I made a plan with the sections that it will contain. I put them in a chronological order and the last section in this list reads acknowledgements. It is last not because it is not important, but rather due to the fact that I was afraid that I if I write it early I will not acknowledge someone who helped me. So now, one day before the submission of my thesis I would like to express my gratitude to all the people who passed from my life during my phd years.

First of all I would like to thank my supervisor Prof. Ralph G. Andrzejak. I want to thank you Ralph because you were not only a scientist but also a teacher. You shared your knowledge and experience with us, you showed us how we make scientific research and write scientific articles. Moreover, you showed us the importance of writing the truth in our articles. In other words, to write all the results the bad and the good ones and to always provide proper scientific explanations. At the same time as a teacher you dedicated a lot of your time showing us with patience the way that we treat the problems that arise in our analysis. Moreover, we, as phd students learned from you not only when you were talking to us in the group and individual meetings, but also when we were observing you in your communication with other professors, when you were inviting students to make projects in our group. You taught us with your eye movements when you were analyzing your own results with a proficient and scientific way. These things do not encompass all the knowledge and experience that you constantly have been providing us. They are just small thankful comments. So I would say thank you for ALL. Thank you from my heart. Moreover, I am very grateful to Prof. Dimitris Kugiumtzis. Dimitris was my MSc thesis supervisor and he was the one who suggested to come here in Barcelona and work with Ralph. Thank you Dimitri for all your guidance and knowledge that you gave me. I would also want to thank Prof. Michael Rosenblum and Prof. Ulrich Parlitz. The concise discussions that we had together in conferences are unforgettable. You transferred me not only knowledge but also enthusiasm for continuing my research. Additionally, I would like to acknowledge Prof. Thomas

Kreuz who kindly hosted me for my research stay in Florence. Vielen Dank Thomas for your positive and welcoming behavior.

Furthermore, I want to thank all the members of my group. Daniel Naro you are my first collaborator who although at the moment of your arrival you were an undergraduate student, you were standing as a phd student. Thank you Daniel! Then came Pau and our group started to increase gradually. Irene and Federico thank you for your love and all the moments that we had together. The scientific and the non-scientific discussions that we had are both in my heart. In the last year of my Phd arrived Cristina, Giulia and Marc. Thank you for all your support, encouragement, help and scientific discussions that we had. I also want to thank our bachelor and master students Raul, Andrea, Minia, Maria, Nico and Javier. Furthermore, I owe many thanks to my officemates Karim, Xenia, Marco, Corne, Jing, Remy and Daniel. Thank you for all the nice moments that we had together and your advice. I would like to specially thank Daniel. Daniel vielen Dank for the mathematical discussions that we had together, for making the cluster a reality, your nice attitude, kindness and support. I am also grateful to all my students. You brought me freshness and happiness. Thank you for all the minisymposia that we organized together in the class, your kindness and support. The fantastic secretaries of our university owe special thanks due to their excellent job that they make in our department. Lydia, Montse, Jana, Joana and Bea muchicimas gracias.

I am also grateful to my friends Nico, Anna and Themis. Your help, guidance, support and encouragement is unforgettable. Moreover, I am grateful to all my friends from my master in computational physics. Although we did parallel our Phd studies in different countries all over the world, we continued to keep in touch and support one each other. So, Taso, Gianni, Dimitra, Eleni, Dora, Antoni and Vicky $\epsilon\upsilon\chi\alpha\rho\iota\sigma\tau\omega$. Here in Barcelona I made very good friends. Maro, Pol, Montserrat, Gabriela, Chrysanthi, Kalpi thank you for all your support! Moreover, I met Mrs. Stavroula and Mr. Taso as well as Mrs. Maria and Mr. Achilles. Thank you for all your love! Your presence gave me the feeling that I have family here in Barcelona.

As in the scientific articles the last author's name is usually the head of the group, I would like to thank the head of the "group" that I belong from the moment that I was born. I would like to thank my parents Zisi and Ermioni for their sacrificed love. This kind of love forgets itself and thinks and wants the best for the others. The others are not only the children but also, the neighbors, the colleagues in the work, the people who are around us with all their differences and characteristics. I love you and I wish that at some moment in my life I will have the same character and attitude as you have. My sisters Anastasia and Dimitra and my brother Dimitri have been my biggest supporters in whatever I have done in my life. Thank you for all your love and encouragements. Although being far from home I know that your thoughts were always with me. I am feeling blessed from God raised up in such family. Thank you from my heart for everything.

Abstract

The characterization of interactions between coupled dynamics from their signals is important for the understanding of real-world systems. The particular aspect of the detection of directional interactions has a central position in the analysis of dynamics. In simple unidirectionally coupled dynamics directional interactions can be achieved by applying data-driven approaches. However, for more complex dynamics the characterization of their directional interactions is not so straightforward. To address this problem we follow a data-driven approach by analyzing signals of pairs and ensembles of non-identical coupled dynamics. In particular, we use a nonlinear state-space approach and a phase-based approach. For the pairs of bidirectionally coupled dynamics, we introduce the notion of the coupling impact that allows us to better reveal the real effect that one dynamics has on the other for different degrees of asymmetry. Furthermore, we show that the coupling and its direction can be detected even for large ensembles of dynamics. Our results demonstrate that directional interactions in complex dynamics can be successfully inferred from the analysis of their signals. Hence, our work shows that the approaches are promising for a reliable detection of directional interactions from real-world signals.

La caracterización de interacciones entre dinámicas acopladas a partir de sus señales, es importante para entender los sistemas del mundo real. Particularmente, la detección de interacciones direccionales tiene un papel fundamental en el análisis de dinámicas. En las dinámicas acopladas unidireccionalemente, las interacciones direccionales pueden lograrse mediante el uso de técnicas dirigidas por datos. Sin embargo, para dinámicas más complejas, la caracterización de sus interacciones direccionales no es tan trivial. Para abordar el tema, hemos utilizado una medida basada en datos analizando señales de pares y grupos de dinámicas acopladas no idénticas. En particular, utilizamos una medida de espacio de estados no linear y una medida basada en fases. Para los pares de dinámicas acopladas bidireccionalmente, presentamos el con-

cepto de impacto de acoplamiento que nos permite desvelar mejor el efecto real que tiene una dinámica sobre la otra con distintos niveles de asimetría. Además, demostramos que el acoplamiento y su dirección pueden ser detectados incluso para grandes conjuntos de dinámicas. Nuestros resultados ponen de manifiesto que las interacciones direccionales en dinámicas complejas pueden ser entendidas satisfactoriamente a partir del estudio de sus señales. Por lo tanto, nuestro trabajo evidencia que estas técnicas son prometedoras para la detección fehaciente de interacciones direccionales de señales del mundo real.

La caracterització de les interaccions entre sistemes dinàmics acoblats a partir de les seves senyals és important per entendre els sistemes del món real. L'aspecte particular de la detecció d'interaccions direccionals té una posició central en l'anàlisis de sistemes dinàmics. En simples dinmiques unidireccionalment acoblades, la direcció d'acoblament es pot detectar mitjançant mètodes basats en la informació dels senyals. Malgrat això, per dinàmiques més complexes, la caracterització de la direcció de l'interacció no és tan trivial. Per adreçar aquest problema, utilitzarem un enfocament basat en la informació de les senyals analitzant senyals de parelles i conjunts de dinàmiques acoblades no idèntiques. En particular, utilitzem mètodes basats en l'espai d'estats i en la fase del sistema. Per parelles de sistemes dinàmics acoblades bidireccionalment, introdum la noció de impacte d'acoblament. Aquest concepte ens permet revelar l'efecte real que un sistema dinàmic fa envers l'altre per diferents graus d'asimetria. A més, ensenyem que l'acoblament i la seva direcció pot ser detectada fins i tot per grans conjunts de sistemes dinàmics. Els nostres resultats demostren que les interaccions direccionals en dinàmiques complexes poden ser detectades amb èxit a partir de l'anàlisis de les seves senyals. Per tant, el nostre treball posa de manifest que les tècniques utilitzades són prometedores per una detecció fiable de les interaccions direccionals dels senyals de sistemes del món real.

Contents

List of Figures

Chapter 1

INTRODUCTION

In nature there are abundant examples of interacting systems that evolve over time. These systems are called dynamics, and the characterization of their interaction is important for the understanding of their behavior. Prominent examples include the interplay between physiological [20, 29, 5, 21], ecological [41] and climate [37, 42] dynamics. In addition, interactions between real-world dynamics like the stock market indexes in economy [23, 39] have been studied in order to better understand their behavior. To understand the interplay of these systems, we want to quantify the degree of their interaction and also to find its direction. In order to achieve this goal many data-driven approaches have been developed. These approaches are applied to the measurements of the dynamics with the aim to infer the connectivity between the coupled dynamics. The data-driven approaches have different modalities and characteristics. They are based on state-space reconstruction [24, 59, 8, 51, 4, 15], phases [54, 66, 58, 27, 28, 30, 31], information theory [60, 43, 44, 74, 19, 32], linear correlation [56, 34, 35], dynamical Bayesian inferrence analysis [64, 67, 68, 57, 17] as well as on neural networks [9, 38], among others.

When the data-driven approaches which aim to characterize directional couplings are developed they are not directly applied to experimental data. Instead, an evaluation on known model dynamics is required. In this way it can be assessed if the approaches are sensitive which means that they

detect the presence of coupling and specific which indicates that the approaches correctly detect the absence of coupling. In this work we use the state-space approach L [15] and the phase-based approach d [54, 27, 28]. These approaches are based on different assumptions and capture different characteristics of the signals. Moreover, it has been shown that in unidirectionally coupled dynamics these approaches successfully capture the strength and the direction of the interaction between the coupled dynamics [54, 15]. In particular, Chicharro and Andrzejak ([15] and references therein) showed that L has better sensitivity and specificity than previous state-space approaches. Moreover, Kraleman et al. [27, 28] proposed an improved method for phase extraction from signals that results in a more accurate estimation of the phase-based approach d.

In this study we want to characterize interactions between more complex dynamics, such as pairs of non-identical bidirectionally coupled dynamics. Furthermore, we investigate if we are able to detect directional interactions between high-dimesional dynamics like pairs of ensembles of non-identical coupled dynamics. When two bidirectionally coupled dynamics are identical symmetric interactions between them can be straightforwardly defined by their coupling strength values [54, 74]. However, this does not hold when the coupled dynamics are non-identical [65, 54]. To address this problem we introduce the notion of the coupling impact [33] that considers apart from the coupling strength the energy of the individual dynamics as expressed through the variance of the signals. We show that the coupling impact better reveals the real effect that one dynamics has on the other for different degrees of asymmetry.

After pairs of coupled dynamics we analyze pairs of ensembles of dynamics. Many real-world dynamics have collective behavior in the sense that they are composed of many interacting units. Moreover, oftentimes the measurements of such dynamics reflect the average activity of the interacting units. Such measurements are called called mean field signals. A characteristic example is the brain dynamics which consists of billions of interacting neurons [25]. Additionally, one type of the brain measurements, the electroencephalographic recordings, reflect the average electrical activity of populations of neurons [13]. Many studies were

carried out for the characterization of synchronization between the interacting units of the ensembles by using their mean field signals [49, 63]. Moreover, a phase-based approach [16] was applied to the mean fields in order to infer the connectivity between interacting ensembles of neural models. Here, we analyze ensembles of coupled dynamics and apply the state-space measure L in order to investigate if it is able to capture directional couplings between the two ensembles. We demonstrate that the strength of the interaction and its direction can be detected even for large ensembles of coupled dynamics. Moreover, we show the advantage of the measure L over its previous version the measure M.

In the beginning of this thesis (Ch. 2) we provide the theoretical concept of dynamics and explain the phase-space and state-space reconstruction. Afterwards, we present the data-driven connectivity measures M, L and d (Ch. 3). In Ch. 4 and 5 we analyze pairs and ensembles of coupled dynamics, respectively. In the end (Ch. 6) we summarize the results of this work.

Chapter 2

DYNAMICS AND SIGNALS

2.1 Dynamical systems

Every system that evolves over time is called dynamics or dynamical system [69]. The dynamics can be natural like the brain or artificial. Artificial dynamics that evolve in continuous time are called continuous and they are often composed by ordinary differential equations. In such cases they can be described by the d-dimensional system

$$\begin{aligned} \dot{x}_1(t) &= f_1(x_1(t), x_2(t), \ldots, x_d(t)), \\ &\vdots \\ \dot{x}_d(t) &= f_d(x_1(t), x_2(t), \ldots, x_d(t)), \end{aligned} \tag{2.1}$$

where t denotes the time, $x_j(t), j = 1, \ldots, d$ are the variables of the dynamics and $\dot{x}_j(t)$ stands for the time derivative of $x_j(t)$. When the functions f_j of the right-hand side of Eqs. (2.1) are linear the dynamics is called linear. Otherwise it is called nonlinear. For a time instant $t_i = i\Delta t, i \in \mathbb{N}$ and $\Delta t \to 0$ an infinitesimal sampling interval, we have an instantaneous state of the dynamics described by Eqs. (2.1). This state is represented by the d-dimensional point $\mathbf{x}(t_i) = (x_1(t_i), x_2(t_i), \ldots, x_d(t_i))$. If we join all these points across all values of time t_i we obtain the trajectory of the dynamics which is located in the

d-dimensional state-space. The trajectory could diverge to infinity or be bounded in a specific space forming a geometrical shape which is called attractor. From the dynamics we take measurements the so-called time series or signals. A time series is a sequence of measurements that are taken from a dynamics at integer multiples of a sampling time Δt [26]. Accordingly, from Eqs. (2.1) ($\dot{\mathbf{x}}(t) = \mathbf{f}(\mathbf{x}(t)),$ where $\mathbf{f} = (f_1, \ldots, f_d)$) we can obtain d scalar time series

$$s_i = h(\mathbf{x}(t_i)),\ t_i = i\Delta t \tag{2.2}$$

with the help of a measurement function h. As an example we provide the Lorenz dynamics [36]

$$\begin{aligned} \dot{x}_1(t) &= 10\,(-x_1(t) + x_2(t)), \\ \dot{x}_2(t) &= 28\,x_1(t) - x_2(t) - x_1(t)\,x_3(t), \\ \dot{x}_3(t) &= x_1(t)\,x_2(t) - \frac{8}{3}\,x_3(t). \end{aligned} \tag{2.3}$$

We integrate the differential equations (Eqs. (2.3)) with the fourth-order Runge-Kutta method. The time step for the integration is 0.005 time units and the sampling interval is $\Delta t = 0.03$ time units. We also apply preiterations in the integration in order to discard transients. In Fig. 2.1 we can see the trajectory of the Lorenz dynamics that forms an attractor in the 3-dimensional state-space. If we project every point of the trajectory on each axis, then we obtain three scalar time series, one for each variable. Fig. 2.2 illustrates the signal that we get from the variable x_1.

Dynamics like the Lorenz (Eqs. (2.3)) are deterministic. In such dynamics when the present state is fixed all the future states are well determined [26]. If this is not the case, they are called stochastic. Stochastic dynamics contain dynamical noise $\xi(t)$ and they can be described by

$$\dot{\mathbf{x}}(t) = \mathbf{f}(\mathbf{x}(t), \xi(t)). \tag{2.4}$$

This means that the noise is intrinsic and each state of the dynamics contains randomness. In other words, the present state of the dynamics does not unambiguously determine its temporal future state. Here, we have to

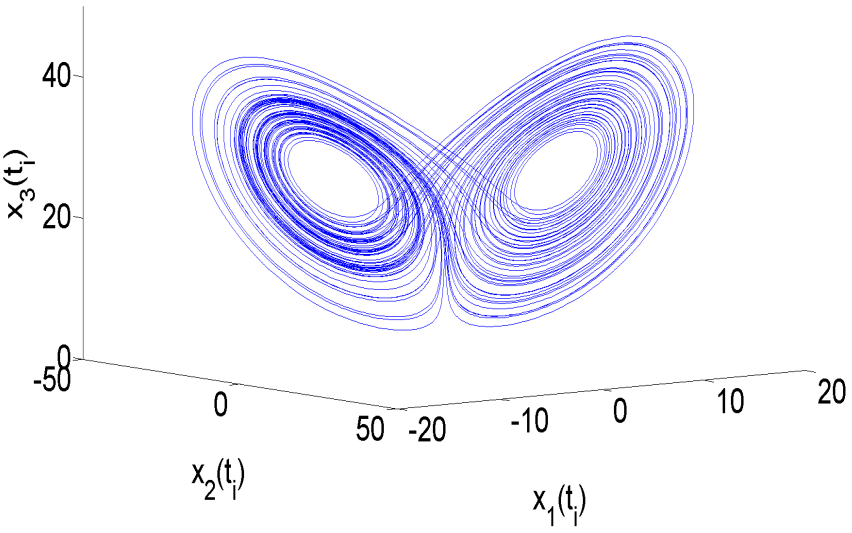

Figure 2.1: The trajectory of the Lorenz dynamics (Eqs. (2.3)) forms an attractor in the 3-dimensional state-space.

underline that when the noise $\xi(t)$ enters only in the measurement then the noise is called observational or measurement noise. If we assume that the dynamics $\dot{\mathbf{x}}(t) = \mathbf{f}(\mathbf{x}(t))$ is deterministic and we contaminate it with observational noise $\xi(t)$ then the measured signal can be described by:

$$s_i = h(\mathbf{x}(t_i), \xi(t_i)),\ t_i = i\Delta t \tag{2.5}$$

Observational noise does not affect the future evolution of the dynamics $\dot{\mathbf{x}}(t) = \mathbf{f}(\mathbf{x}(t))$ which remains deterministic. In other words, observational noise depends rather on the imprecision during the measurement process and it is defined as the difference between the actual state of the system and the observed state.

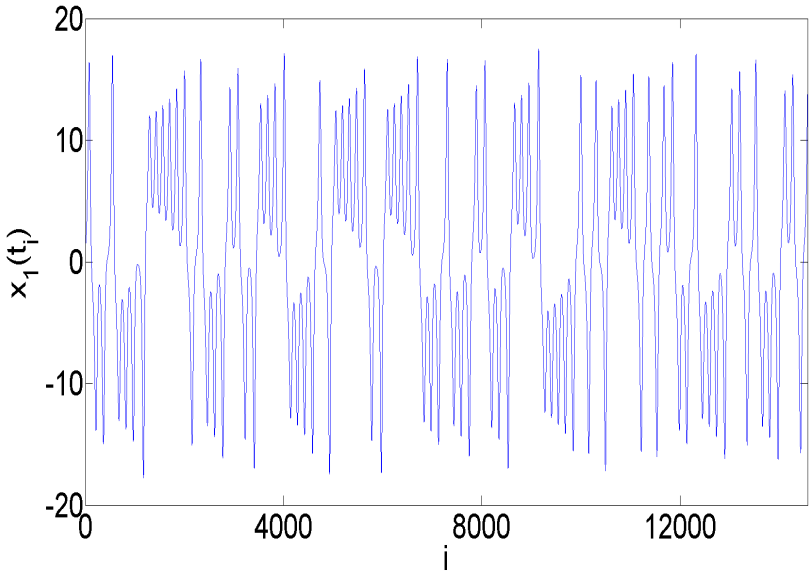

Figure 2.2: The signal that results from the projection of the x_1 component of the Lorenz attractor on the x_1 axes of Fig. 2.1.

2.2 Characterization of interactions between dynamics

In coupled dynamics the most simple type of interaction can occur between a pair of dynamics, while complex interactions occur between ensembles of dynamics. In the first case the interaction can be unidirectional, when only one dynamics influences the other, or bidirectional where both dynamics exchange information. In the case for which ensembles of dynamics interact, their interplay is more complex. Here, interactions could take place not only within the elements (i.e. dynamics) of the same ensemble but also between the elements of different ensembles. For the characterization of this interplay the signal analysis techniques that have been developed analyze the measurements from the dynamics. The analysis that is done with these approaches can be bivariate where only

two signals are used [24, 59, 8, 51, 4, 15, 54, 66, 60, 43, 44, 74, 56] or multivariate when more signals are available [58, 19, 32, 31, 35, 17]. In this thesis we use two bivariate approaches: the state-space approach L [15] as well as the phase-based approach d [54, 27, 28]. The measure L directly uses the the amplitudes of the measurements and it is based on the reconstruction of the dynamics' state-space. On the other hand, the measure d utilizes phase variables that are extracted from the signals. Therefore, we continue by explaining the notion of the state space reconstruction (Sec. 2.3) and the phase variable (Sec. 2.4).

2.3 State space reconstruction

The state space reconstruction is the basic notion that the measure L is based on. Moreover, it is commonly used in nonlinear signal analysis techniques ([15] and referencies therein). In Sec. 2.1 we explained that the signals are measurements from dynamics. In real-world experiments we only have signals (e.g. electrocardiogram) and the information about the dynamics that produced the signal is limited. With the state space reconstruction we aim to construct from the measured signal an estimate of the state space of the underlying unknown dynamics. To achieve this we use the method of delays that was introduced by the embedding theorem of Takens [71]. This theorem assumes that the measured signal reflects all the degrees of freedom of the underlying stationary dynamics. Moreover, it requires that the measurement function h (Eq. (2.2)) is invertible and the length of the noise-free signal is infinitely long. If we have a measured scalar signal $s_i,\ i = 1, \ldots, N$ we built m-dimensional embedding vectors $\mathbf{s}_i$ ($m \geq 2D + 1$, ([26] and references therein) D is the dimension of the original attractor) with delay τ

$$\mathbf{s}_a = (s_a, s_{a-\tau}, s_{a-2\tau}, \ldots, s_{a-(m-1)\tau}),\ a = (m-1)\tau + 1, \ldots, N. \quad (2.6)$$

The real-world signals are not infinitely long and noise is always present. Moreover, the dimension D of their underlying dynamics is in generall unknown. Thus, in order to obtain a good estimation of the underlying

dynamics we have to adjust the values of m and τ. The selection of the proper m and τ values is a study by itself. The embedding delay τ is often selected with regard to the first zero of autocorrelation function or the first local minimum of the mutual information function [26]. For the embedding dimension m, the method of false nearest neighbors is often used among others [26]. In practice the selection of m and τ is on dependence of the variability of the results of the connectivity measure that we apply. We use first a broad range of m and τ values and for each combination of them we apply the connectivity measure (e.g. the measure L). For some values of m and τ the results for L will be similar. Finally, we select one of these m, τ values for which the connectivity measure had similarity on its values.

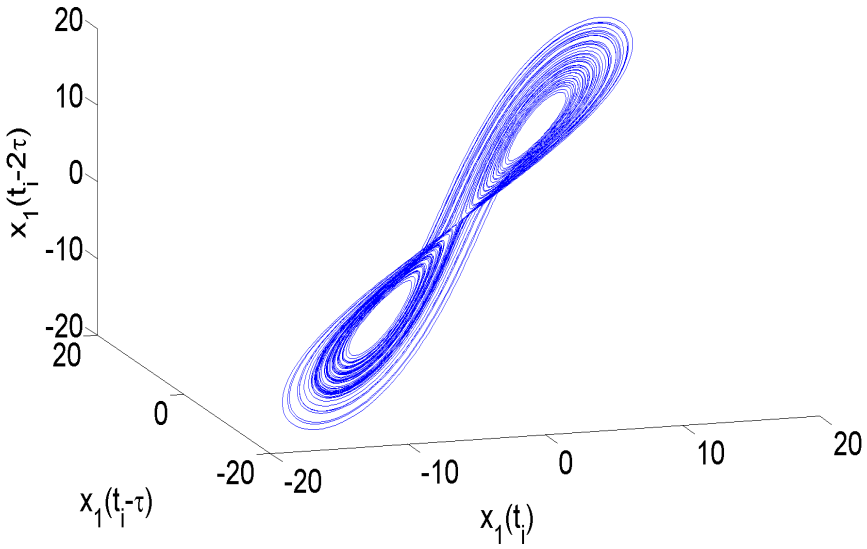

Figure 2.3: The reconstructed state space from the x_1 variable of the Lorenz dynamics (Eqs. (2.3)) with $m = 3$ and $\tau = 5$.

As an example of the state space reconstruction we provide the re-

construction of the Lorenz dynamics (Eqs. (2.3)). For optical reasons we use an embedding of $m = 3$ and a time delay of $\tau = 5$ sampling times. If we use the signal from the x_1 component (Fig. 2.2) we can build 3-dimensional embedding vectors with delay $\tau = 5$. The resulted state space is depicted on Fig. 2.3. We can see that the shape of the attractor that is formed is topologically similar [2] to the original one (Fig. 2.1).

2.4 Phase variable

Dynamics (Eqs. (2.1)) that have a periodic solution $\mathbf{x}(t_i) = \mathbf{x}(t_i + T)$, where T denotes the period, form in their state-space closed attractive trajectories which are called limit cycles. A characteristic example is the van der Pol dynamics

$$\begin{aligned} \dot{x}_1(t) &= x_2(t), \\ \dot{x}_2(t) &= 0.2(1 - x_1^2(t))x_2(t) - 0.9025\, x_1(t). \end{aligned} \tag{2.7}$$

For the integration of this dynamics we use the Euler method with time step 0.01π time units and sampling interval $\Delta t = 0.1\pi$ time units. In Fig. 2.4 we can clearly see the limit cycle which is formed in the state space. The motion of the point that is moving along the limit cycle can be described by a variable ϕ that is called phase. In other words, the phase variable ϕ parameterizes the motion of the point along the limit cycle. The phase ϕ grows monotonically in the direction of the motion and gains 2π in each cycle. Moreover, its growth is uniform in time such

$$\dot{\phi}(t) = \omega, \tag{2.8}$$

where $\omega = 2\pi/T_0$ governs the natural frequency of the dynamics.

2.4.1 Extraction of phases from measurements

An important topic is how we can extract phase variables ϕ (Eq. (2.8) from data. This process is done in two stages. In the first stage we obtain

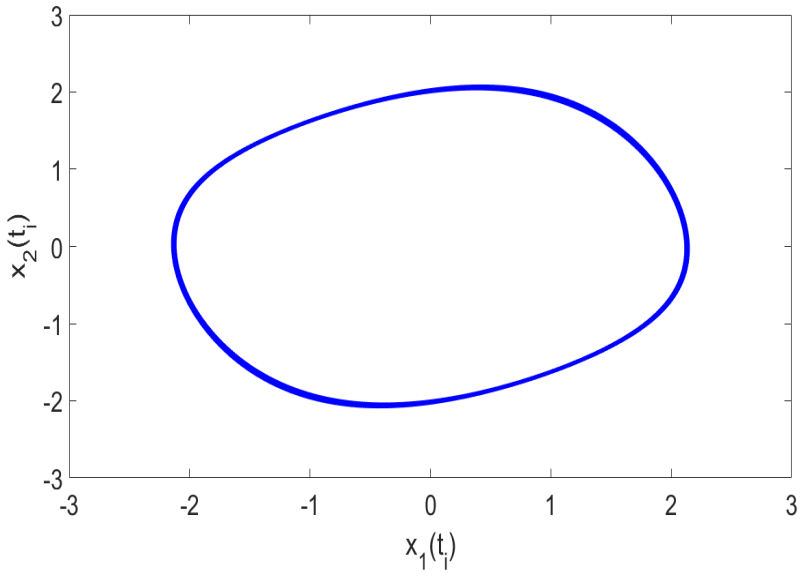

Figure 2.4: The limit cycle of the van der Pol dynamics (Eqs. (2.7)) in the 2-dimensional state-space.

preliminary phases θ which are called protophases (from the Greek word $\pi\rho\omega\tau os$ (protos = first) and $\phi\alpha\sigma\eta$ (phasi = phase)) [27, 28]. In general there are many ways to extract protophases from data [48]. Here, we follow the analytic signal approach [22] based on the Hilbert transform. The analytic signal $z(t)$ is a complex function of time and gives the instantaneous protophase and amplitude of a signal $x(t)$. It is defines as:

$$z(t) = x(t) + i\,\tilde{x}(t) = A(t)e^{i\theta(t)} \tag{2.9}$$

where, $\tilde{x}(t)$ is the Hilbert transform of $x(t)$

$$\tilde{x}(t) = \frac{1}{\pi} p.v. \int_{-\infty}^{\infty} \frac{x(t')}{t - t'} \mathrm{d}t', \tag{2.10}$$

and $p.v.$ stands for the Cauchy principal value. Then, the instantaneous protophase is given by

$$\theta(t) = \arctan\frac{\tilde{x}(t)}{x(t)}. \tag{2.11}$$

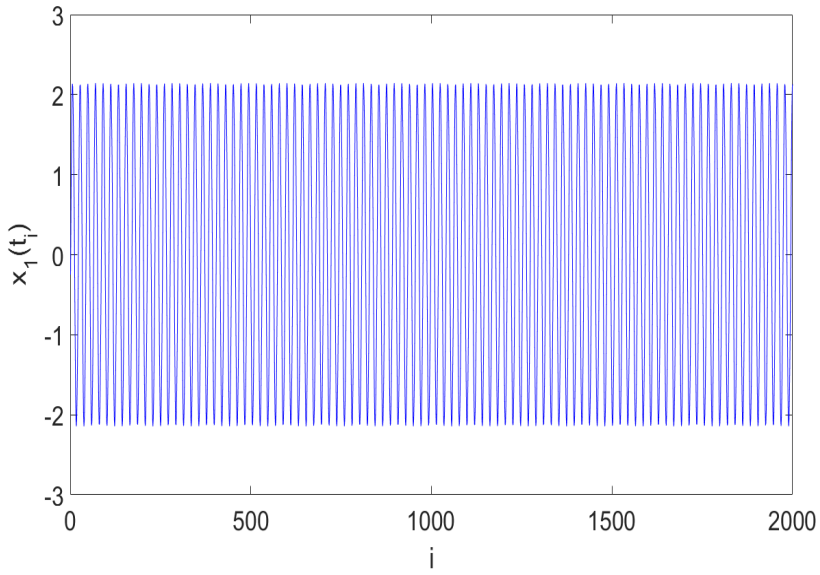

Figure 2.5: The signal of the x_1 variable of the van der Pol dynamics (Eqs. (2.7)).

The Hilbert transform applies a time shifting of $\pi/2$ to the signal $x(t)$ while the phase spectrum remains unchanged. Thus, by ploting the signal $x(t)$ on dependence on its Hilbert trasform we can obtain points that follow circular rotations around an origin. If we consider the signal (Fig. 2.5) from the x_1 variable of the van der Pol dynamics (Eqs. (2.7)), then by applying a two dimensional embedding based on the Hilbert transform (Fig. 2.6) we can obtain the protophases. In Fig. 2.6 we can clearly see that the protophases are well-defined. This means that all cycles rotate

around the same origin (here this is the point (0,0)) and $x(t)$ as well as its Hilbert transform $\tilde{x}(t)$ do not vanish simultaneously [48]. On the contrary, when the signal has many fluctuations on its amplitudes (Fig. 2.7) the cycles in the Hilbert embeddding do not all rotate around the same origin (Fig. 2.8) and therefore the protophases are not well-defined. We have to underline that in the calculation of the instantaneous protophases of a signal we should always take into account the boundary effect. Practically, this means that when we apply the Hilbert embedding on a signal we have to eliminate its first and last part (approximately 10 periods [48]).

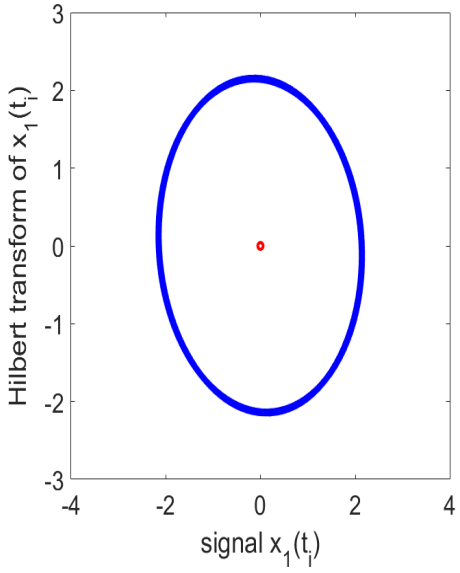

Figure 2.6: Well defined instantaneous phases. The Hilbert transform of $x_1(t)$ versus the signal $x_1(t)$ of the van der Pol dynamics (Eqs. (2.7)). The red circle denotes the origin.

The protophase θ that we obtain from the analytic signal approach (Eq. (2.9)) does not in general have the properties of phase ϕ (Eq. (2.8)) [27, 28]. Although θ is 2π-periodic it does not always grow linearly in

time but obeys $\dot{\theta}(t) = f(\theta(t))$. Moreover, it depends on the method (e.g. Hilbert transform) that we used to extract it from the signal. Therefore, the second stage of the process of extracting phase variables from data is to transform the protophase θ to the genuine phase ϕ (Eq.(2.8)). This transformation reads

$$\phi(t) = \theta(t) + 2\sum_{n=1}^{n_F} \mathrm{Im}\Big[\frac{S_n}{n}(\exp^{in\theta(t)} - 1)\Big], \tag{2.12}$$

where $S_n = N^{-1}\sum_{i=1}^{N} \exp^{-in\theta(t_i)}$ are coefficients of the Fourier expansion of the probabilitity density function (p.d.f.) of θ. This p.d.f. is calculated from the signal of protophases $\theta(t_i)$, $i = 1, \ldots, N$. The optimal number of Fourier nodes n_F is selected according to a study done by Tenreiro [72, 31]. The transformation that we apply on θ is invertible and it is neither an interpolation nor a filtering. Figure 2.9 depicts the phase ϕ that we obtain from the x_1 variable of the van der Pol dynamics (Eqs. (2.7)) after applying the Hilbert transform and the transformation on the protophase θ.

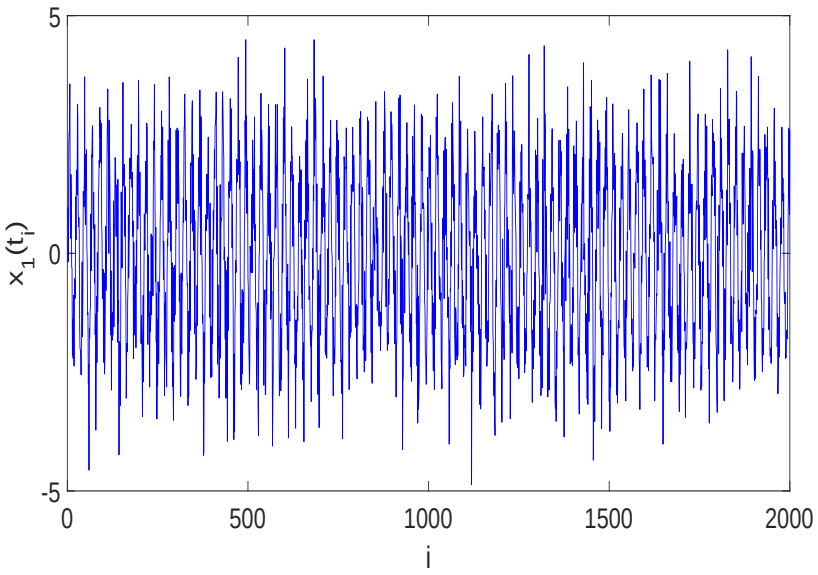

Figure 2.7: The signal $x_1(t_i)$ of Fig. 2.5 contaminated with 60% Gaussian noise.

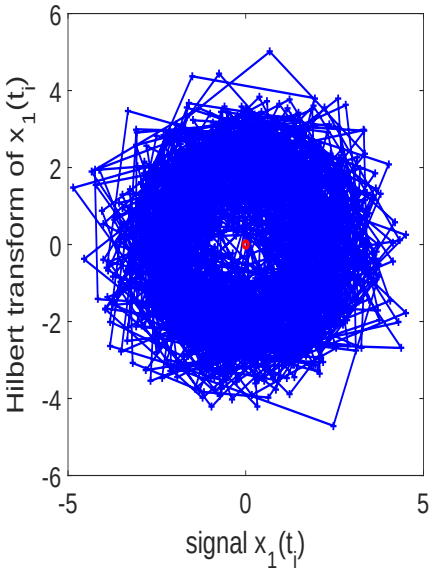

Figure 2.8: Not well-defined instantaneous phases. The Hilbert transform of the noisy signal $x_1(t)$ (Fig. 2.7) versus the noisy signal $x_1(t)$. The red circle denotes the origin.

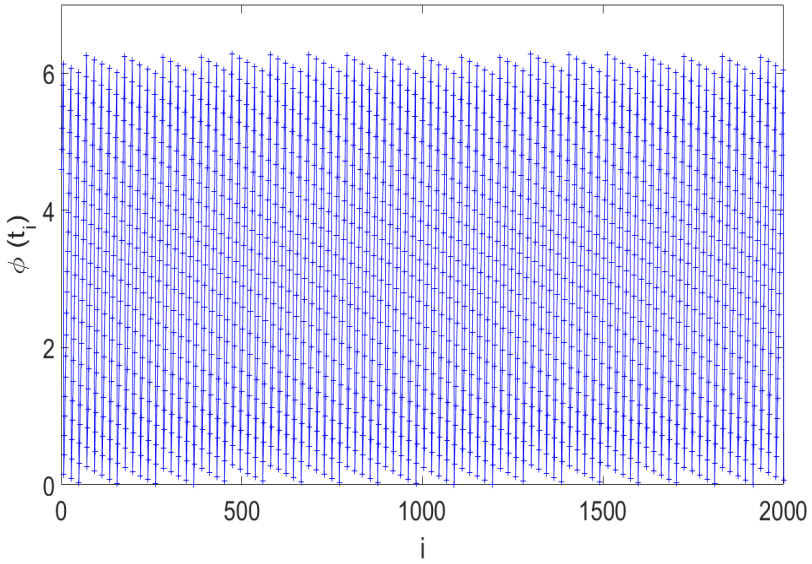

Figure 2.9: The genuine phases $\phi(t)$ of the signal $x_1(t)$ (Fig. 2.5) of the van der Pol dynamics (Eqs. (2.7)).

Chapter 3

BIVARIATE CONNECTIVITY MEASURES

3.1 Introduction

In this chapter we explain the bivariate, data-driven approaches that we follow for the characterization of connectivity between two coupled dynamics X and Y. These approaches aim to reveal not only the strength of interaction between X and Y but also its direction. They belong to two categories in the sense whether they assume or not the existence of a model of the underlying dynamics. In Sec. 3.2 we present the non model-based approaches which are the state space measures M[4] and L [15]. Afterwards in Sec. 3.3 we provide the model-based approach which is the phase-based directionality index d [54, 27, 28]. All these measures assume stationarity in the sense that the generating dynamics have no explicit time dependence. Moreover, strong coupling between X and Y should not be present. When two dynamics are synchronized in the amplitude or in the phase domain, then the detection of the interaction is no longer possible [54, 65, 44, 15, 74, 19].

3.2 State space approaches

The state-space approaches M [4] and L [15] are bivariate directional interdependence measures. Chicharo and Andrzejak [15] showed that in unidirectionally coupled dynamics L prevails over M. In our study we will use the measure L and only in Ch. 5 we will apply the measure M in order to to show its lower accuracy over L. The measure L was successfully applied to experimental data, like neuronal [1] and musical data [45]. Moreover, it was applied to electroencephalographic recordings from epilepsy patients and it was shown that in combination with surrogates it is able to localize the epileptic focus [3] as well as to assess the nonlinear interdependence in the brain [6]. Both measures utilize the amplitudes of the measured signals and they require the dynamics to be aperiodic. They are based on two notions. The first one is the state space reconstruction (Sec. 2.3) and the second one is the asymmetric state similarity criterion. Here, we explain asymmetric state similarity criterion and afterwards we present the measures.

3.2.1 The asymmetric state similarity criterion

The second notion that the state-space measures M and L use is the asymmetric state similarity criterion. According to this criterion, if the dynamics X is unidirectionally coupled to the dynamics Y ($X \rightarrow Y$) then the probability that spatial close neighbors in the state space of Y are mapped to spatial close neighbors in the state space of X is higher than in the opposite direction [24, 59, 8, 50].

Let us graphically observe the mapping between close neighbors of model dynamics. We consider a unidirectional interaction between two Lorenz dynamics, where X is the driving dynamics and Y is the driven one. We evaluate two cases. In the first one there is coupling from X to Y dynamics. In the second one the two dynamics are uncoupled. The

equations for the driving Lorenz read

$$\begin{aligned}\dot{x}_1(t) &= 10\,(-x_1(t) + x_2(t)),\\ \dot{x}_2(t) &= 30\,x_1(t) - x_2(t) - x_1(t)\,x_3(t),\\ \dot{x}_3(t) &= x_1(t)\,x_2(t) - \frac{8}{3}\,x_3(t).\end{aligned} \tag{3.1}$$

and for the driven dynamics the equations are:

$$\begin{aligned}\dot{y}_1(t) &= 10\,(-y_1(t) + y_2(t)),\\ \dot{y}_2(t) &= 35\,y_1(t) - y_2(t) - y_1(t)\,y_3(t) + \epsilon_x\,(x_2(t) - y_2(t)),\\ \dot{y}_3(t) &= y_1(t)\,y_2(t) - \frac{8}{3}\,y_3(t).\end{aligned} \tag{3.2}$$

If we use the signals of their second components x_2, y_2 and we make a reconstruction of their state spaces with $m = 3, \tau = 5$ we can clearly see that in the case of coupling (Fig. 3.1), spatial close neighbors in the driven Lorenz dynamics are mapped to spatial close neighbors in the driving one. On the contrary, when the coupling between the dynamics is absent (Fig. 3.2), spatial close neighbors in the driven Lorenz dynamics are not mapped to spatial close neighbors in the driving dynamics.

Summarizing we can say that when a relation $X \to Y$ exists, then close neighbors in the Y dynamics are mapped to close neighbors in the X dynamics. The mapping in the other direction (i.e from $X \to Y$) also holds to a weaker degree. The quantification of this mapping is the basic feature that gives the directionality between two coupled X and Y dynamics. We underline that in order to define the predominant direction of the interaction between X and Y one has to consider the mapping between close neighbors in both directions ($X \to Y$ and $Y \to X$) [15]

3.2.2 The measures M and L

We now review the algorithms for the calculation of M [4] and L [15]. We start with the measure M. Suppose that we have two simultaneously measured signals $x_i, y_i, i = 1, \ldots, N$ derived from the dynamics X and Y, respectively. Using the method of delays [71], we

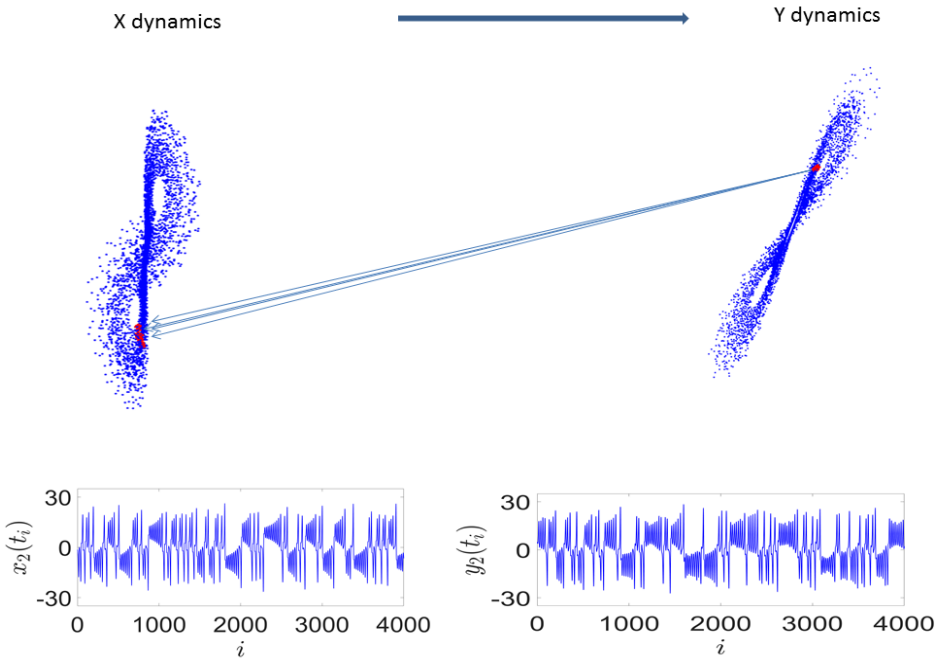

Figure 3.1: Mapping of close neighbors in the coupled Lorenz dynamics. Close states in the driven dynamics Y are mapped to close states in the driving dynamics X.

reconstruct the X and Y dynamics with embedding delay τ and embedding dimension m. The embedding vectors for the X dynamics are $\mathbf{x}_a = (x_a, x_{a-\tau}, \ldots, x_{a-(m-1)\tau})$ and for the Y dynamics they are $\mathbf{y}_a = (y_a, y_{a-\tau}, \ldots, y_{a-(m-1)\tau})$, where $a = h+1, \ldots, N$ and $h = (m-1)\tau$.

With $u_{a,b}$ and $w_{a,b}$, $b = 1, \ldots, k$ we denote the time indexes of the k spatially nearest neighbors of x_a and y_a, respectively. In order to avoid the selection of temporally close neighbors, we apply a Theiler window, W [73]. This means that the time indices of all neighbors of $\mathbf{x}_a$ and y_a should satisfy $|u_{a,b} - a| > W$ and $|w_{a,b} - a| > W$, respectively. For each reference embedding vector $\mathbf{x}_a$, the mean squared Euclidean distance to its k nearest neighbors is $R_a^k(X) = \frac{1}{k}\sum_{a=h+1}^{N} |\mathbf{x}_a - \mathbf{x}_{u_{a,b}}|^2$. Similarly,

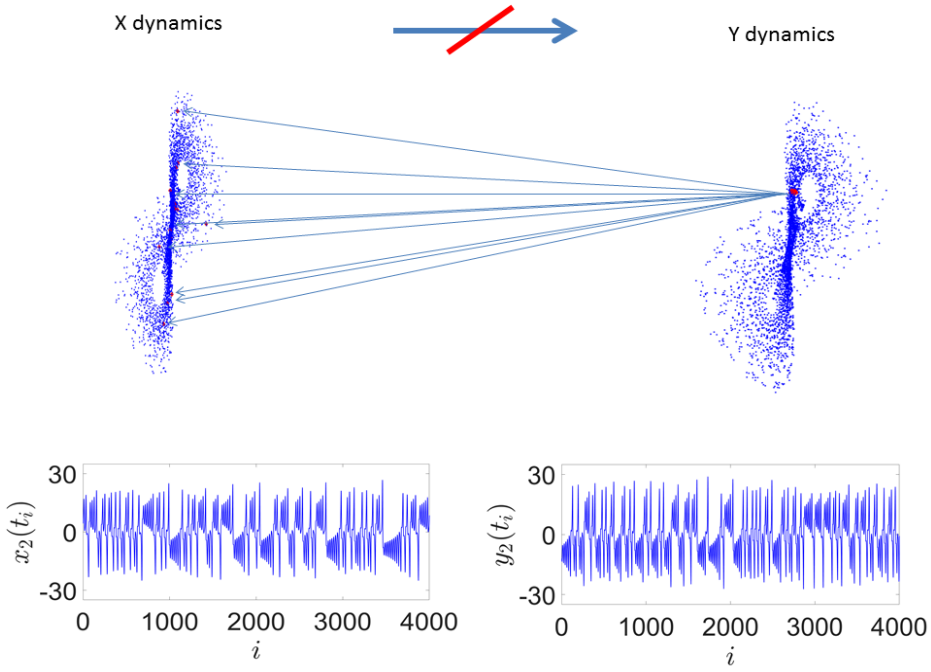

Figure 3.2: Mapping of close neighbors in the uncoupled Lorenz dynamics. Close states in the "driven" dynamics Y are not mapped to close states in the driving dynamics X.

the Y-conditioned distance is $R_a^k(Y) = \frac{1}{k}\sum_{a=h+1}^{N} |\mathbf{x}_a - \mathbf{x}_{w_{a,b}}|^2$. The mean distance of $\mathbf{x}_a$ to all the other embedding vectors $\mathbf{x}_o$, $o = h+1, \ldots, N$, $o \neq a$ is $R_a(X) = \frac{1}{N_a - 1}\sum_{a=h+1}^{N} |\mathbf{x}_a - \mathbf{x}_o|^2$, where $N_a = N - h$ holds for the range $W < a < N - W + 1$. Below and above the bounds of this range N_a increases linearly and reaches $N_a = N - W - 1$ at $a = h+1$ and $a = N$. Considering these distances the interdependence $M(X|Y)$ from the X to the Y dynamics is defined by:

$$M(X|Y) = \frac{1}{N-h}\sum_{a=h+1}^{N} \frac{R_a(X) - R_a^k(X|Y)}{R_a(X) - R_a^k(X)}. \tag{3.3}$$

The algorithm for the measure L is very similar with the one of the

measure M. Loosely speaking we can say that L is M with ranks. In other words if we transform the distances of Eq. (3.3) to ranks we will obtain L. Therefore, instead of having $R_a^k(X)$ we now have the constant $G_a^k(X) = \frac{k+1}{2}$ which denotes the mean value of the ranks of the k nearest neighbors of each reference point $\mathbf{x}_a$. Moreover, the quantity $G_a(X) = \frac{N_a+1}{2}$ substitutes the quantity $R_a(X)$ and denotes the average rank between $\mathbf{x}_a$ and all the others $\mathbf{x}_o$ embedding vectors. Finally, for each reference point of the X dynamics, $\mathbf{x}_a$ we calculate the Y-conditioned mean rank $G_a^k(X|Y) = \frac{1}{k}\sum_{b=1}^{k} g_{a,w_{a,b}}$. The term $g_{a,w_{a,b}}$ denotes the rank that the distance between $\mathbf{x}_a$ and $\mathbf{x}_{w_{a,b}}$ takes in a sorted ascending list of all the distances between $\mathbf{x}_a$ and all $\mathbf{x}_o$. $L(X|Y)$ is defined by:

$$L(X|Y) = \frac{1}{N-h}\sum_{a=h+1}^{N}\frac{G_a(X) - G_a^k(X|Y)}{G_a(X) - G^k(X)}. \tag{3.4}$$

With A we denote M or L. To assess the interdependence $A(Y|X)$ from Y to X we follow the corresponding above processes by exchanging the roles of X and Y. Accordingly, we define $\Delta A = A(X|Y) - A(Y|X)$ for the characterization of the predominant direction of interaction between the X and Y dynamics.

When we have identical synchronization ($Y = X$) then $G_a^k(X|Y) = G_a^k(X)$, and $L(X|Y) = 1$. If there is an interaction from $X \to Y$ then $0 < L(X|Y) < 1$. When the dynamics X and Y are independent, then $G_a^k(X|Y) \approx G_a(X)$ and the values of $L(X|Y)$ are distributed symmetrically around zero. Similar values are obtained by the measure M but Chicharro and Andrzejak [15] showed that L has better sensitivity and specificity than M [14].

3.3 Phase-based approach

The bivariate directional phase-based approach d [54, 27, 28] aims at the reconstruction of pairs of coupled phase dynamics through an analysis of the instantaneous phases and the instantaneous frequencies. It is based

on the assumption that the dynamics can be described by a phase variable and this phase variable can be reconstructed from the measured signal. Moreover, the interacting dynamics should be self-sustained. Later, this approach was extended to characterize interactions in networks of coupled oscillators [30, 31]. It was successfully applied not only in bivariate but also in multivariate model systems and to experimental data [54, 53, 11, 16, 40, 27, 28, 30, 29, 31]. In this Section we provide the general concept of the phase-based approach. Moreover, we explain how to use the phase variables that are extracted from measurements (Sec. 2.4.1) in order to reconstruct the phase dynamics.

3.3.1 General concept of the directionality index d

The phase-based approach utilizes the fact that an autonomous periodic oscillator can be characterized by a phase ϕ which grows uniformly in time (Eq. (2.8)). For the case of two coupled dynamics X, Y we have to take into account their interaction. Accordingly, they can be described by

$$\begin{aligned} \dot{\phi_x} &= \omega_x + q_x(\phi_x, \phi_y), \\ \dot{\phi_y} &= \omega_y + q_y(\phi_y, \phi_x), \end{aligned} \tag{3.5}$$

where $\phi_{x,y}$ are the phase variables, $\omega_{x,y}$ govern the natural frequencies and $q_{x,y}$ are the coupling functions which are 2π-periodic with respect to their arguments [54, 48]. The interaction between the X and Y dynamics can be quantified with the norms of the coupling functions $q_{x,y}$. The interaction from $Y \rightarrow X$ and vice versa can be characterized by $c_x = \frac{||q_x||}{\omega_x}$ and $c_y = \frac{||q_y||}{\omega_y}$, respectively. Finally, the directionality index d [54] is calculated as

$$d = \frac{c_y - c_x}{c_x + c_y}. \tag{3.6}$$

For uncoupled dynamics zero values of d are expected. With increasing unidirectional coupling from X to Y positive values of d with an upper bound of 1 are obtained. For the opposite coupling direction negative values are attained with a limit of -1. The sign of d can be used to conclude the predominant coupling direction. Additionally, equal estimates

of interaction in both directions between X and Y result in zero values of d.

3.3.2 Reconstruction of phase dynamics

In Sec. 3.3.1 we presented the general concept of the phase-based directionality index d. Here we will describe how we can reconstruct the phase dynamics (Eqs. (3.5)) by using the measurements of the underlying dynamics. Assume that we have two simultaneously measured time series x_i, y_i, $i = 1, \ldots, N$ that correspond to the dynamics X and Y respectively. We first extract the genuine phases ϕ_x, ϕ_y from the signals x_i, y_i respectively (Sec. 2.4.1) and afterwards we numerically calculate their time derivatives. According to Eqs. (3.5) the derivatives of the phases are 2π-periodic functions of the phases. Hence, we represent the right hand side of Eqs. (3.5) as double Fourier series of order p

$$\begin{aligned}\dot{\phi}_{x,y} &= \omega_{x,y} + q_{x,y}(\phi_x, \phi_y) + \xi_{x,y} \\ &= \sum_{v=-p}^{p} \sum_{l=-p}^{p} Q_{v,l}^{(x,y)} e^{i(v\phi_x + l\phi_y)} + \xi_{x,y}. \end{aligned} \tag{3.7}$$

Here, we include noise terms $\xi_{x,y}$ that are always present in real-wold data. The coefficients $Q_{v,l}^{(x,y)}$ are estimated by means of a least mean square fit. From the coefficients $Q_{0,0}^{(x,y)}$ we estimate the natural frequencies $\omega_{x,y}$ that are denoted by $\bar{\omega}_{x,y}$ [27, 28]. The norms of the coupling functions are given by

$$\mathrm{E}^{(x,y)} = \Big(\sum_{v=-p}^{p} \sum_{l=-p}^{p} |Q_{v,l}^{(x,y)}|^2 \Big)^{1/2}. \tag{3.8}$$

From the summation and for both X and Y dynamics the case for which $m = l = 0$ (estimated natural frequencies) is excluded. In the end the norms $\mathrm{E}^{(x,y)}$ of the coupling functions are normalized by the estimated natural frequencies in order to obtain the influence of one dynamics on

the other,

$$c_x = \frac{\mathrm{E}^{(x)}}{\bar{\omega}_x}, \quad c_y = \frac{\mathrm{E}^{(y)}}{\bar{\omega}_y}. \tag{3.9}$$

Finally, by substituting Eqs. (3.9) in Eq. (3.6) we obtain the directionality index d [10].

Chapter 4

INTERACTIONS BETWEEN TWO COUPLED DYNAMICS

4.1 Introduction

In the Introduction (Ch. 1) of this thesis we mentioned that many data-driven approaches successfully detect interactions between unidirectionally coupled dynamics. However, a characterization of bidirectional interactions is not so straightforward. Hence, in this chapter we will investigate whether we can characterize interactions between non-identical bidirectionally coupled dynamics. We summarize our study [33] published in the peer -reviewed journal Physical Review E and we closely follow its text. Let us consider two bidirectionally coupled dynamics X and Y the evolution of which is described by the time-dependent state space vectors $\mathbf{x(t)} = \{x_1(t), x_2(t), \ldots, x_d(t)\}$ and $\mathbf{y}(t) = \{y_1(t), y_2(t), \ldots, y_{d'}(t)\}$, respectively. Their equations of motion have the form:

$$\begin{aligned} \dot{\mathbf{x}}(t) &= F(\mathbf{x}(t),\ f(y_{j'}(t), x_j(t), \epsilon_y)), \\ \dot{\mathbf{y}}(t) &= G(\mathbf{y}(t),\ g(x_j(t), y_{j'}(t), \epsilon_x)). \end{aligned} \tag{4.1}$$

The function f represents an interaction from the Y to the X dynamics with coupling strength ϵ_y. The x_j and $y_{j'}$ components are involved in this interaction, with $j = 1, \ldots, d$ and $j' = 1, \ldots, d'$. Analogously, the function g represents the interaction from the X to the Y dynamics with coupling strength ϵ_x.

The relevant components in this bidirectional interaction between X and Y are the coupling strength values as well as the variables of the dynamics which are contained in the coupling terms. Moreover, X and Y can be identical or non-identical. When X and Y are identical their coupling strengths as well as their variables are the same. However, this does not hold when X and Y are non-identical. Thus, a question that results reads: Is it possible to define a symmetric interaction between non-identical coupled dynamics? To address this question, we follow a data-driven approach by analyzing pairs of signals derived from coupled model systems. Particularly, we use the directional state space measure L (Sec. 3.2) and the phase-based directionality index d (Sec. 3.3).

Rosenblum and Pikovsky [54] applied the phase-based directionality index d in a system of bidirectionally coupled dynamics X and Y. They found that when the coupled dynamics X and Y are almost identical, equal estimates of the interdependence in both directions, as judged by their phase-based approach, were correctly obtained for equal ϵ_x, ϵ_y values. In other words, symmetric interactions between two identical or almost identical X and Y dynamics can be defined directly from the coupling strength values. On the other hand, Rosenblum and Pikovsky [54] indicated that when the X and Y dynamics are non-identical, equal estimates of the interdependence in both directions are obtained for different ϵ_x, ϵ_y values. Hence, the coupling strengths are not by themselves enough to characterize an interaction to be symmetric.

To address this asymmetry in coupled dynamics we introduce in this study the notion of coupling impact. The coupling impact takes into account both the coupling strength and the energy of the individual dynamics. As a data-driven estimator of this energy we use the variance of the signals. In particular we use the variance of the variables through which the dynamics are coupled. This is straightforward, since it is this vari-

ance in combination with the coupling strength that reflects the energy which is transmitted from one dynamics to the other. We determine the coupling strength values as well as the coupling impact values for which the two directional connectivity measures L and d judge the interaction to be symmetric. In Sec. 4.2 we present the coupled dynamics that we use and provide the information for the implementation of the connectivity measures. Afterwards, we introduce the coupling impact (Sec. 4.3) and we present the results (Sec. 4.4). Finally, in Sec. 4.5 we discuss the conclusions of this study.

4.2 Methods

4.2.1 Coupled dynamics

We analyze pairs of bidirectionally coupled deterministic chaotic dynamics as well as noisy limit-cycle oscillators. The pairs of chaotic dynamics comprise identical, almost identical and non-identical coupled Lorenz, Rössler and Rössler-Lorenz dynamics. We also use noisy non-identical van der Pol oscillators as an example of limit-cycle oscillators. As we mentioned in Sec. 3.1 we want to avoid synchronization between the X and Y dynamics. Therefore, we restrict our analysis to coupling strength values that do not result in a functional relation between the amplitudes (for the chaotic dynamics) and between the phases (for the limit-cycle oscillators). Without loss of generality, we fix the coupling strength from X to Y, denoted by ϵ_x, and we vary the coupling strength from Y to X, denoted by ϵ_y. Our first dynamics are coupled Lorenz:

$$\begin{aligned}
\dot{x}_1(t) &= 10\,(-x_1(t) + x_2(t)) + \epsilon_y\,(y_1(t) - x_1(t)),\\
\dot{x}_2(t) &= R_x\,x_1(t) - x_2(t) - x_1(t)\,x_3(t),\\
\dot{x}_3(t) &= x_1(t)\,x_2(t) - \frac{8}{3}\,x_3(t),
\end{aligned} \tag{4.2}$$

and

$$\begin{aligned}
\dot{y}_1(t) &= 10\,(-y_1(t) + y_2(t)) + \epsilon_x\,(x_1(t) - y_1(t)),\\
\dot{y}_2(t) &= R_y\,y_1(t) - y_2(t) - y_1(t)\,y_3(t),\\
\dot{y}_3(t) &= y_1(t)\,y_2(t) - \frac{8}{3}\,y_3(t).
\end{aligned} \tag{4.3}$$

Here, the coupling strength from $X \to Y$ is fixed to $\epsilon_x = 1.2$ and the coupling strength ϵ_y from $Y \to X$ runs from 0.5 to 2.48 in steps of 0.02. All dynamics depend on some parameters. Therefore, we can control the degree of asymmetry between the dynamics by changing these parameters. For the coupled Lorenz dynamics, we vary the values of R_x, R_y from 48 to 54 in steps of 2. Taking all the possible combinations of R_x, R_y values we obtain 12 pairs of non-identical and 4 pairs of identical coupled Lorenz dynamics. We analyze the signals that are obtained from the components x_1, y_1.

For the integration of all chaotic dynamics we use the the fourth-order Runge-Kutta method. For the coupled Lorenz dynamics (Eqs. (4.2)-(4.3)), the step size for the integration is 0.005 time units and the sampling interval is $\Delta t = 0.03$ time units. As a consequence, every rotation period of the Lorenz dynamics contains approximately 20 samples which we consider as an appropriate sampling of the dynamics [65]. We always use random initial conditions and in order to discard transients we apply preiterations in the numerical integration. The signals that we use for the analysis consist of 4096 points and they correspond to 200 basic periods approximately.

For the coupled Rössler dynamics [49] the equations read

$$\begin{aligned}
\dot{x}_1(t) &= -\omega_x\,x_2(t) - x_3(t) + \epsilon_y(y_1(t) - x_1(t)),\\
\dot{x}_2(t) &= \omega_x\,x_1(t) + 0.25\,x_2(t),\\
\dot{x}_3(t) &= (x_1(t) - 8.5)\,x_3(t) + 0.4,
\end{aligned} \tag{4.4}$$

and

$$\begin{aligned}
\dot{y}_1(t) &= -\omega_y\, y_2(t) - y_3(t) + \epsilon_x\,(x_1(t) - y_1(t)),\\
\dot{y}_2(t) &= \omega_y\, y_1(t) + 0.25\, y_2(t),\\
\dot{y}_3(t) &= (y_1(t) - 8.5)\, y_3(t) + 0.4.
\end{aligned} \tag{4.5}$$

The mean frequencies ω_x, ω_y take the values $\omega_x, \omega_y = \{0.9, 0.905, 1.045, 1.05\}$. Thus, the 16 possible combinations between the ω_x, ω_y values can be classified as follows. We obtain 4 pairs of identical (e.g. $\omega_x = 0.9, \omega_y = 0.9$), 4 pairs of almost identical (e.g. $\omega_x = 0.9, \omega_y = 0.905$) and 8 pairs of non-identical coupled Rössler dynamics (e.g. $\omega_x = 0.9, \omega_y = 1.05$). We fix $\epsilon_x = 0.02$ and the ϵ_y values run from 0.01 to 0.0298 in steps of 0.0002. The integration step is 0.05 time units, and the sampling interval is set to $\Delta t = 0.3$ time units, again resulting in approximately 20 points per cycle. We use the variables x_1, y_1 as observables.

We also study the Rössler-Lorenz dynamics an example where the dynamics do not only have different parameters but they also have different structure:

$$\begin{aligned}
\dot{x}_1(t) &= 10(-\omega_x\, x_2(t) - x_3(t)) + \epsilon_y(y_2(t) - x_1(t)),\\
\dot{x}_2(t) &= 10(\omega_x\, x_1(t) + 0.25\, x_2(t)),\\
\dot{x}_3(t) &= 10((x_1(t) - 8.5)\, x_3(t) + 0.4),
\end{aligned} \tag{4.6}$$

and

$$\begin{aligned}
\dot{y}_1(t) &= 10\,(-y_1(t) + y_2(t)),\\
\dot{y}_2(t) &= R_y\, y_1(t) - y_2(t) - y_1(t)\, y_3(t) + \epsilon_x\,(x_1(t) - y_2(t)),\\
\dot{y}_3(t) &= y_1(t)\, y_2(t) - \frac{8}{3}\, y_3(t).
\end{aligned} \tag{4.7}$$

We vary the ω_x values as well as the R_y values in the same ranges that we used for the coupled Rössler and coupled Lorenz dynamics, namely $\omega_x = \{0.9, 0.905, 1.045, 1.05\}$ and $R_y = \{48, 50, 52, 54\}$. Therefore, across all the combinations of ω_x and R_y we obtain 16 pairs of coupled Rössler-Lorenz dynamics. The fixed coupling strength from X

to Y is $\epsilon_x = 0.55$ and the varied coupling strength from Y to X is $\epsilon_y = 0.3/1.02^{i-1},\ i = 1, \ldots, 100$. The step size for the integration is 0.005 time units and the sampling interval is $\Delta t = 0.03$ time units. Since we use the same Rössler and Lorenz dynamics as in the previous coupled dynamics, we multiply the right hand side of the Rössler equations with the factor of 10 to continue to have approximately 20 points per cycle for both dynamics. In this dynamics we analyzed the signals from the x_1, y_2 components.

The limit-cycle oscillators consist of van der Pol oscillators which read

$$\begin{aligned} \ddot{x}(t) &= 0.2(1 - x^2(t))\dot{x}(t) - \omega_x^2 x(t) + \epsilon_y(y(t) - x(t)) + \eta_x, \\ \ddot{y}(t) &= 0.2(1 - y^2(t))\dot{y}(t) - \omega_y^2 y(t) + \epsilon_x(x(t) - y(t)) + \eta_y, \end{aligned} \tag{4.8}$$

where η_x, η_y are independent white Gaussian noises with zero mean and correlation functions $\langle \eta_{x,y}(t)\eta_{x,y}(t')\rangle = 2D_{x,y}\delta(t - t')\delta_{x,y}$. For the integration of this type of dynamics we use the Euler method with step size $dt = 0.01\pi$ time units. The variables x, y are used as observables. The sampling interval is 0.1π time units again resulting in approximately 20 points per cycle for each oscillator. The values of the frequencies ω_x, ω_y vary in steps of 0.01 in the ranges $[1.09, 1.12]$ and $[0.88, 0.91]$ respectively. Accordingly, we obtain 16 pairs of non-identical coupled oscillators. For the aforementioned ranges of frequency we fix the standard deviation of noise, the so-called noise level $\xi_{x,y} = \sqrt{2D}_{x,y}$ to 0.04. We also vary the values of the noise $\xi_{x,y}$ in the range [0.02, 0.05] in steps of 0.01, while the frequencies are fixed to $\omega_x = 1.1$ and $\omega_y = 0.9$. Concerning the coupling values, ϵ_x is set to 0.05, and the ϵ_y values vary in steps of 2×10^{-4} in the range $[0.04002, 0.06]$. Like for the chaotic dynamics we limit the range of the coupling values such that we do not have synchronization.

4.2.2 Implementation of connectivity measures

As we already mentioned, we use in our analysis the connectivity measures L (Sec. 3.2) and d (Sec. 3.3). Both of them require for their calculation the regulation of some parameters. Concerning the measure L, we need to adjust the embedding dimension m, the embedding delay

τ, the number of the nearest neighbors k as well as the Theiler correction W. In a pre-analysis we scanned the ranges $k = [3, 5, 10, 15, 20]$, $m = [4, 5, 6, 7, 8, 9]$ and $\tau = [4, 5, 6, 7, 8, 9]$ sampling times. For all the possible combinations between k, m and τ the values of $\Delta L = L(X|Y) - L(Y|X)$ were similar for $k = [3, 5, 10]$, $m = [4, 5, 6]$ and $\tau = [4, 5, 6]$. Therefore, without performing any kind of optimization, we set the values of k, m and τ to the middle value of these ranges. In other words, we set the parameters of L: $k = 5$ nearest neighbors, embedding dimension $m = 5$ and embedding delay $\tau = 5$ sampling times. For the Theiler window we use $W = 15$. Like described in Sec. 4.2.1 we sample all our dynamics such they have approximately 20 samples per cycle. Accordingly, for the parameters τ and W which are in units of time we can use the same values across all dynamics. The source code resources that we used for the calculation of L can be found in [14].

Concerning the phase-based directionality index d we first need to specify the way for the calculation of the derivatives of the phases. We here use the central finite difference and we set the order p of the Fourier expansion (Eq. (3.7)) to 10. Afterwards, we need to specify the way for the calculation of the norms of the coupling functions. In our study, we use the trapezoidal method. We underline, that one can also follow different methods either for the calculation of the phase derivatives or for the norms of the coupling functions. The source code resources that we use for the measure d can be found in [10].

4.3 Coupling strength and coupling impact

In Sec. 4.1 we discussed the fact that the coupling strength values are not by themselves enough to define symmetric interactions in pairs of non-indetical X to Y dynamics . Instead, in order to define a symmetric interaction between X to Y we also have to consider the energy of the variables through which the coupling is conveyed from one dynamics to the other. In this study we propose the notion of the coupling impact as a quantity that takes into account both the coupling strengths and the

variables' energy. As a data-driven estimator of the variables' energy we use the variance of their corresponding signals. Accordingly, the coupling impact γ_x from X to Y dynamics is given by

$$\gamma_x = \frac{\epsilon_x}{\sigma_y^2}, \tag{4.9}$$

where ϵ_x is the coupling strength from $X \rightarrow Y$ and σ_y^2 is the variance of the signal that corresponds to the variable of the Y dynamics which is contained on the coupling term. For the coupling impact γ_y of the other direction $Y \rightarrow X$, we exchange the roles of the x and y components in Eq. (4.9).

What is the relation between the values of the coupling strength and between the values of the coupling impact when there is a symmetric interaction in the coupled X and Y dynamics as estimated by L or d? In other words, what is the relation between the ϵ_x, ϵ_y values as well as the one between the γ_x, γ_y values for which we obtain $\Delta L = 0$ or $d = 0$?

We carry out an analysis in two stages. We start by describing the process we follow for the chaotic dynamics that we analyze with the measure $\Delta L = L(X|Y) - L(Y|X)$. At first, we pair the fixed value of the coupling strength ϵ_x with a range of 100 values of ϵ_y. The exact range of ϵ_y is determined in a pre-analysis such that in its intermediate range, and given ϵ_x, we obtain equality in the values of L in both directions (Fig. 4.1a). For each pair of dynamics and for each of the 100 sets of the coupling strength (ϵ_x, ϵ_y) we generate 500 independent realizations. In Fig. 4.1b we show the mean values of ΔL across the 500 realizations in dependence on the ratio $r_\epsilon = \epsilon_y/\epsilon_x$ of the coupling strength values. As a consequence of the adjustment of the ϵ_y range, the curve of ΔL crosses zero. In order to estimate the abscissa of the zero-crossing point ($\Delta L = 0$), we fit a third-order polynomial on the curve of the mean values of ΔL using the Brent-Dekker method [12]. The resulting abscissa value is denoted by $r_{\epsilon o}$. In other words, $r_{\epsilon o}$ is the approximated value of ϵ_y/ϵ_x for which there is a symmetric interaction between the X and Y dynamics as judged by the measure L. We illustrate the second stage of our analysis in Fig. 4.2. We plot the mean values of the measure ΔL not in dependence on the ratio

of the coupling strength values $r_\epsilon = \epsilon_y/\epsilon_x$, but in dependence on the ratio of the coupling impact values $r_\gamma = \gamma_y/\gamma_x$. We denote by $r_{\gamma o}$ the abscissa of the point for which we have $\Delta L = 0$. Similarly, for the limit-cycle oscillators we follow exactly the same process, but instead of ΔL we use the directionality index $d = (c_y - c_x)/(c_x + c_y)$.

If we get $r_{\epsilon o} = 1$ this would mean that equal estimates of the interaction between the X and Y dynamics as judged by the measure ΔL (or d) are obtained for equal coupling strength values. Analogously, $r_{\gamma o} = 1$ means that symmetric interaction in the coupled X and Y dynamics is obtained for equal coupling impact values. In order to quantify deviations of $r_{\epsilon o}$ and $r_{\gamma o}$ from one, we define the quantities $\rho_\epsilon = \ln(r_{\epsilon o})$ and $\rho_\gamma = \ln(r_{\gamma o})$.

4.4 Results

We start by illustrating the influence of the asymmetry between the dynamics and the coupling on the variances of the signals. We do this since the variance is the basic component of the coupling impact values. Thus we inspect the relation between the ratio of the coupling strength values $r_\epsilon = \epsilon_y/\epsilon_x$ and the ratio of the variance of the signals $r_v = \sigma_y^2/\sigma_x^2$ across different pairs of Lorenz dynamics (Fig. 4.3). For coupled identical dynamics with equal coupling strength values ($r_\epsilon = 1$), the r_v ratio is 1, correctly reflecting the symmetry of the dynamics and the coupling. For increasingly non-identical dynamics, the r_v ratio gradually diverges from the one obtained for identical dynamics. In addition, for any degree of asymmetry between the dynamics, r_v covaries with r_ϵ.

We now consider strongly asymmetric coupled Lorenz dynamics (Eqs. (4.2)-(4.3) for $R_x = 48$, $R_y = 54$). The coupling strength ϵ_x from $X \to Y$ dynamics is fixed. As a consequence the values of $L(X|Y)$ form an almost horizontal line (Fig. 4.1a). In contrast, since the ϵ_y coupling strength from Y to X dynamics is increasing, so do the values of $L(Y|X)$ (Fig. 4.1a). The graphs in Fig. 4.1b and Fig. 4.2 show the resulting $\Delta L = 0$ values. In each panel, however, the abscissa is scaled differently.

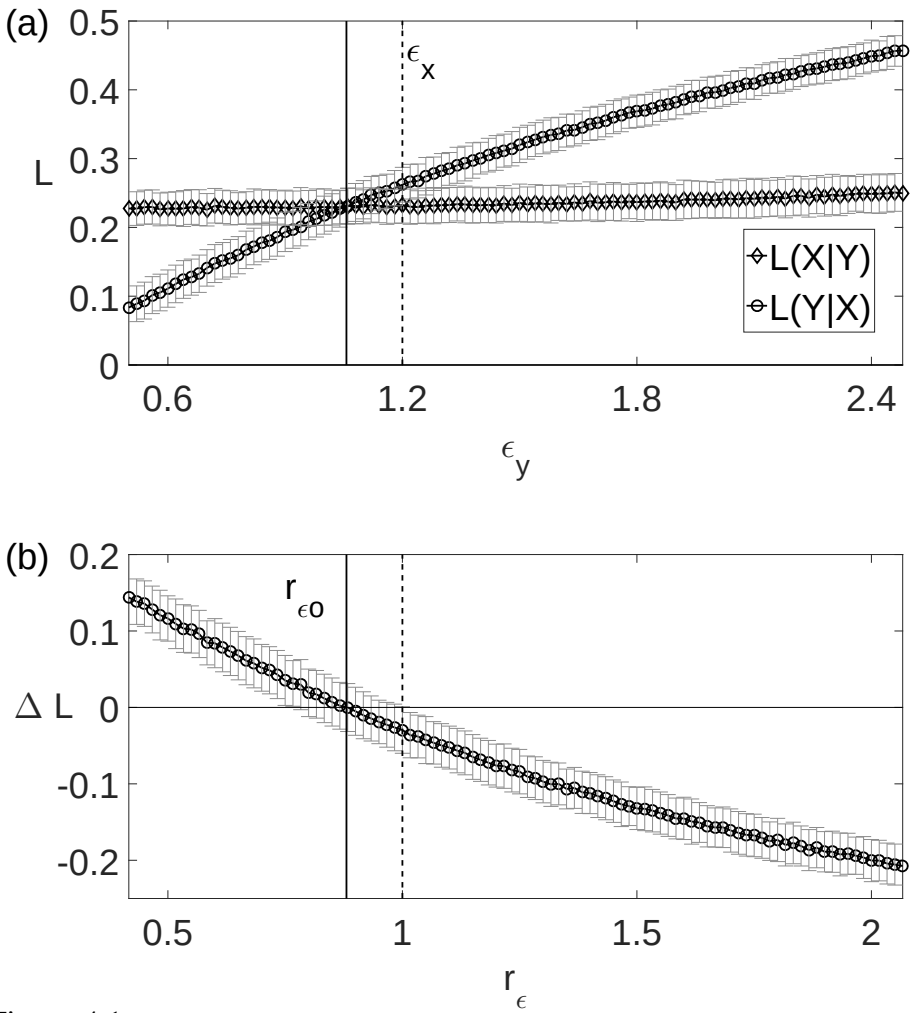

Figure 4.1: The coupling strength does not detect a symmetric interaction in strongly asymmetric coupled Lorenz dynamics. Values of L and ΔL for the coupled Lorenz dynamics ($R_x = 48, R_y = 54$). The error bars depict the mean $\pm$ one standard deviation across 500 independent realizations. In (a) we depict values of $L(X|Y), L(Y|X)$ in dependence on the coupling strength ϵ_y. The vertical dashed line marks the fixed coupling strength $\epsilon_x = 1.2$ from $X \to Y$. In (b) the $\Delta L = L(X|Y) - L(Y|X)$ values are shown in dependence on the ratio of the coupling strength values $r_\epsilon = \epsilon_y/\epsilon_x$. In panel (b) the dashed vertical line highlights the abscissa value of one. The black solid line in (a) marks the crossing point of $L(X|Y), L(Y|X)$ whereas in (b) the solid line stands for the $r_{\epsilon o}$ value.

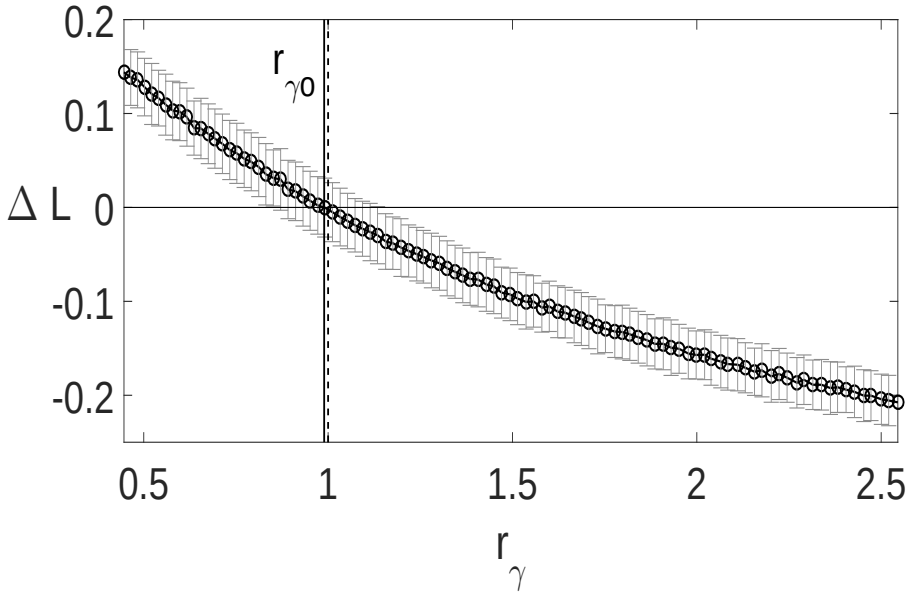

Figure 4.2: The coupling impact detects a symmetric interaction in strongly asymmetric coupled Lorenz dynamics. Values of $\Delta L = L(X|Y) - L(Y|X)$ in dependence on the ratio of the coupling impact values $r_\gamma = \gamma_y/\gamma_x$ for the Lorenz dynamics of Fig. 4.1. Here, the dashed vertical line highlights the abscissa value of one, whereas the solid line stands for the $r_{\gamma o}$ value.

We use ϵ_y in Fig. 4.1a, r_ϵ in Fig. 4.1b, and r_γ in Fig.4.2. Nonetheless, by construction, the crossing point of $L(X|Y)$ and $L(Y|X)$ in Fig. 4.1a and the zero crossing of $\Delta L = 0$ in Figs. 4.1b and 4.2 all have approximately the same relative position with regard to the abscissa limits. These lines are all positioned in the 29th data point. However in Fig. 4.2 the distance between pairs of subsequent points is not constant but depends on the ratio of variances. The ratio of variances in turn depends on the ϵ_y (see again Figs. 4.1, 4.2)

When the degree of interdependence is the same in both directions, as judged by $\Delta L = 0$, the corresponding ratio $r_{\epsilon o}$ of the coupling strength values is different from 1 (Fig. 4.1b). On the other hand, when we use the ratio r_γ of the coupling impact values, for $\Delta L = 0$ the $r_{\gamma o}$ value is almost

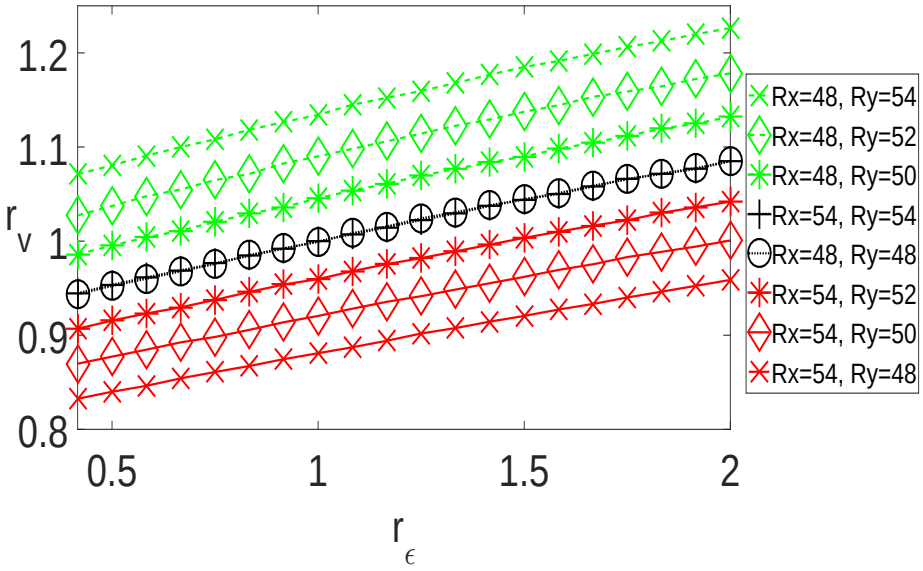

Figure 4.3: Both the asymmetry and the coupling strength of the dynamics affect the variance of the signals. Mean values of the ratio of the variances of the signals $r_v = \sigma_y^2/\sigma_x^2$ in dependence on the ratio of the coupling strength values $r_\epsilon = \epsilon_y/\epsilon_x$. Each curve corresponds to a different coupled Lorenz dynamics with the R_x and R_y values specified in the legend.

equal to 1 (Fig. 4.2). This means that equal estimates of interdependence ($\Delta L = 0$) are obtained for unequal coupling strength values ($r_{\epsilon o} \neq 1$), but for almost equal coupling impact values ($r_{\gamma o} \approx 1$).

We now turn to the effect of the degree of asymmetry of the coupled dynamics on the quantities $\rho_\epsilon = \ln(r_{\epsilon o})$ and $\rho_\gamma = \ln(r_{\gamma o})$ (Figs. 4.4-4.6). We start with the coupled Lorenz dynamics (Eqs. (4.2)-(4.3) for all the set of R_x, R_y values). For pairs of identical dynamics we obtain zero values of ρ_ϵ (Fig. 4.4a). In contrast, for pairs of non-identical dynamics we obtain non-zero values of ρ_ϵ. We also find that an increase in the asymmetry of the dynamics leads to an increase in the absolute values of ρ_ϵ (Fig. 4.4a). In contrast, the use of coupling impact renders the resulting values of ρ_γ to be almost zero for both identical and non-idetical bidirectionally

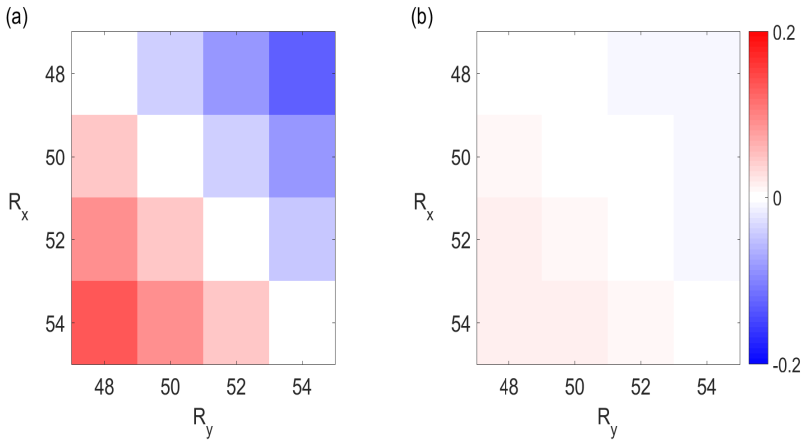

Figure 4.4: The coupling impact correctly detects a symmetric interaction for the coupled deterministic Lorenz dynamics. Values of ρ_ϵ (a) and ρ_γ (b).

coupled Lorenz dynamics (Fig. 4.4b). Similar findings are obtained for the coupled Rössler dynamics (Eqs.(4.4)-(4.5)) for all the set of ω_x, ω_y values) as can be seen in Figs. 4.5a, 4.5b. Again we find that zero values of ρ_ϵ and ρ_γ are obtained for all the pairs of identical dynamics. These results also hold for pairs of almost identical dynamics (top left and bottom right blocks of Figs. 4.5a, 4.5b). Concerning the pairs of non-identical dynamics we obtain non-zero values of ρ_ϵ (Fig. 4.5a). On the other hand, the values of ρ_γ are almost zero (Fig. 4.5b).

We continue with an example of coupled dynamics with different structure given by the Rössler and Lorenz dynamics (Eqs. (4.6)-(4.7)). Since these dynamics are completely different, the ρ_ϵ quantity takes non-zero values (Fig. 4.6a) for all the pairs of dynamics. Moreover, these values are higher than the ones of the coupled Lorenz (Fig.4.4a) and Rössler dynamics (Fig. 4.5a). Despite the strong asymmetry between the coupled

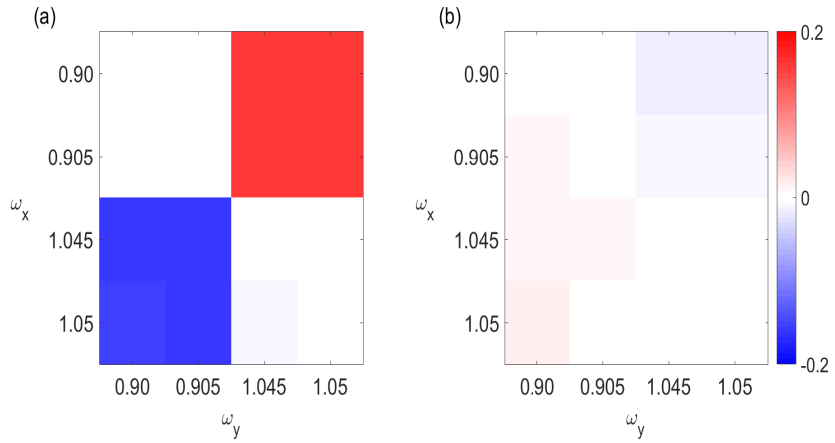

Figure 4.5: Same as Fig. 4.4 but for the coupled Rössler dynamics.

dynamics the use of coupling impact successfully results in values of ρ_γ that are very close to zero (Fig. 4.6b).

In order to assess the accuracy of our results we divide the 500 independent realizations that we made for each pair of dynamics in 5 groups of 100 realizations each. For every group we repeat the analysis as described in Sec. 4.3 and we determine the corresponding ρ_ϵ and ρ_γ values. Their mean value and ranges for the Lorenz, Rössler and Rössler-Lorenz dynamics are shown in Figs. 4.7, 4.8 and 4.9 respectively. The small magnitude of these ranges illustrates that our estimates of ρ_ϵ and ρ_γ are reliable.

We now study limit-cycle oscillators. We follow the exact same procedure like the three chaotic dynamics, but instead of the measure L we use the directionality index d. In particular, we assure that the estimates ρ_ϵ and ρ_γ are of comparably high accuracy as the one obtained for the chaotic dynamics. For all the pairs of non-identical van der Pol oscilla-

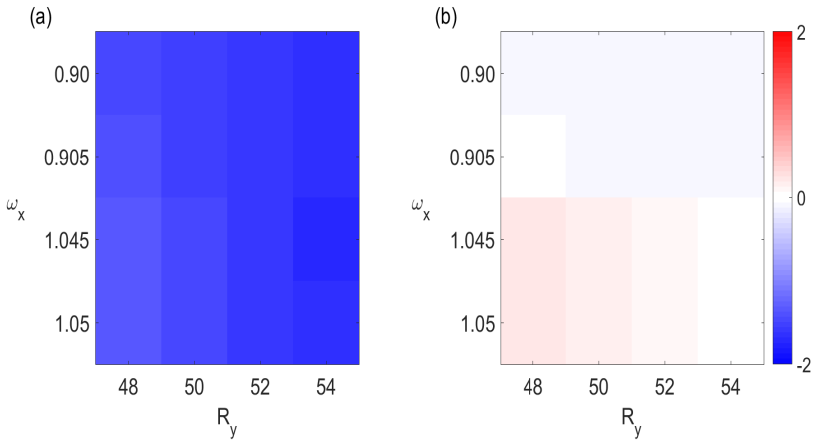

Figure 4.6: Same as Fig. 4.4 but for the coupled Rössler-Lorenz dynamics.

tors (Eqs. (4.8) with $\xi_{x,y} = 0.04$) the values of ρ_ϵ diverge from zero (Fig. 4.10a). Again the more asymmetry between the frequencies ω_x, ω_y of the oscillators the higher absolute values of ρ_ϵ we get. In contrast, the use of coupling impact results in values of ρ_γ close to zero (Fig. 4.10b). We also study the role of noise on the coupling impact. For this purpose, we fix $\omega_x = 1.1, \omega_y = 0.9$ and we vary the noise levels ξ_x, ξ_y from 0.02 to 0.05 in steps of 0.01. In general higher values of noise lead to higher absolute values of ρ_ϵ (Fig. 4.11a). On contrary, the use of coupling impact ends in values of ρ_γ very close to zero (Fig. 4.11b).

4.5 Discussion

In this study we proposed the notion of the coupling impact as a way to define symmetric interactions between non-identical bidirectionally coupled dynamics. For this purpose we followed a data-driven approach by

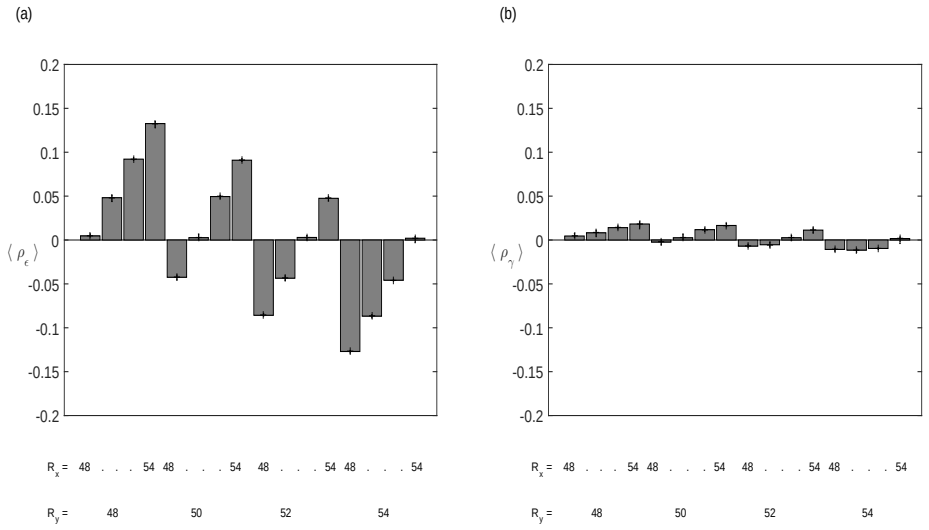

Figure 4.7: High accuracy of the estimation of the coupling strength and coupling impact values. Mean values of ρ_ϵ (a) and ρ_γ (b) for the coupled Lorenz dynamics obtained across five sets of 100 realizations each. The error bars depict the corresponding ranges.

analyzing signals from pairs of coupled dynamics. In order to characterize the interdependence between the interacting dynamics we used the state space measure L [15] as well as the phase-based directionality index d [54, 27, 28]. These measures estimate the strength and direction of the interaction between two dynamics X and Y. At first, we showed that in identical and almost identical bidirectionally coupled dynamics, equal estimates of the interdependence in both directions as judged by L or d are obtained for equal or almost equal values of the coupling strength. This finding is in accordance with expectation and previous findings [54, 74] as it reflects the symmetry between the dynamics in this setting. On the other hand, we showed that in non-identical bidirectionally coupled dynamics equal estimates of interdependence in both directions are obtained

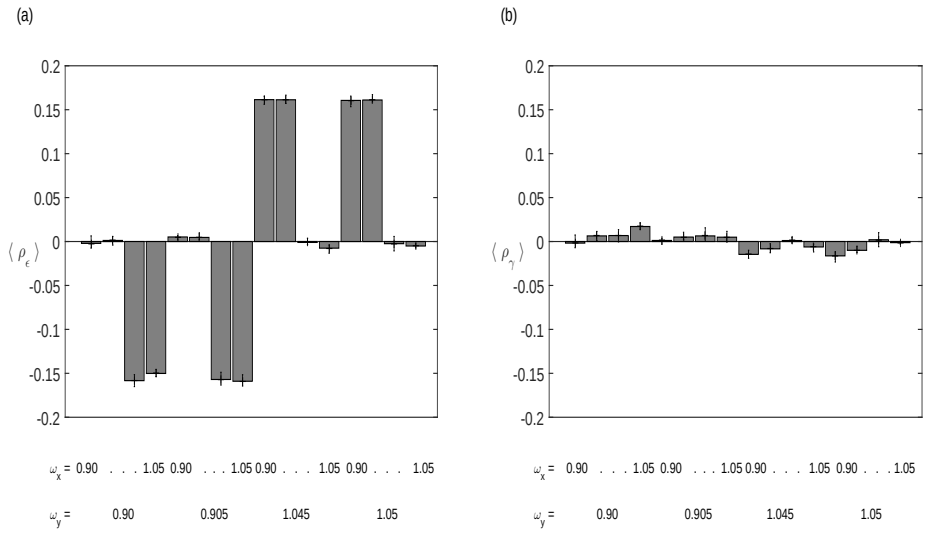

Figure 4.8: Same as Fig. 4.7, but for the coupled Rössler dynamics.

for unequal values of the coupling strength. In other words, in the case of non-identical coupled dynamics, if the coupling strength from the dynamics X to the dynamics Y is stronger than in the opposite direction, this does not always imply that also the interaction from X to Y is higher than for the opposite direction. These findings do not reflect a peculiarity of L or d but are consistent with results of previous studies [54, 65] which used state space [65] and phase-based [65, 54] approaches for the characterization of interaction between bidirectionally coupled dynamics. For increasingly different coupled dynamics, equal estimates of the interaction between the dynamics are obtained for increasingly different coupling strength values. Therefore, the coupling strength values do not determine by themselves the real impact that one dynamics exerts on the other.

In order to address this problem we here introduced the notion of the coupling impact. The coupling impact takes into account not only the

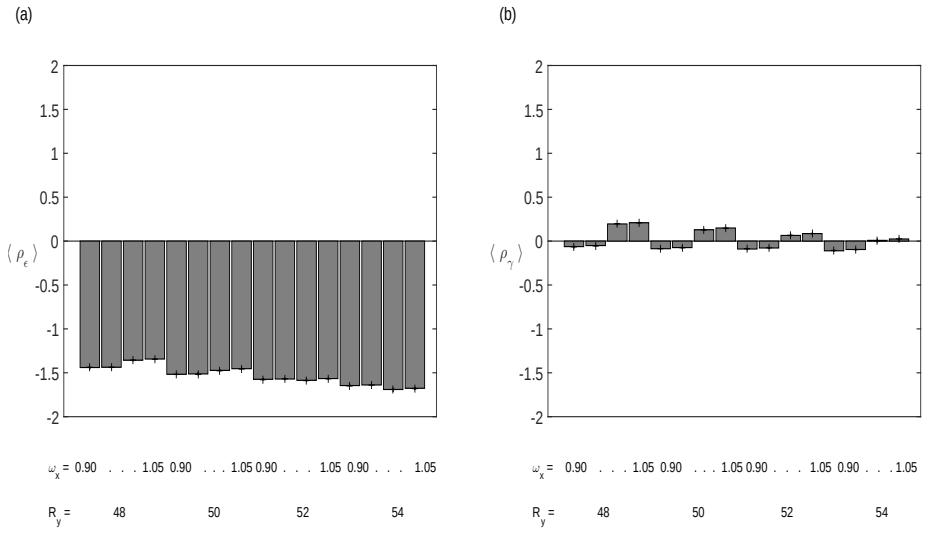

Figure 4.9: Same as Fig. 4.7, but for the coupled Rössler-Lorenz dynamics.

coupling strength between the dynamics but also the energy of the individual dynamics. As an estimator of this energy we used the variance of the signal that corresponds to the variable through which the dynamics are coupled. We found that equal estimates of interdependence in both directions are obtained for approximately equal coupling impact values, regardless of the asymmetry between the coupled dynamics. Hence, this approach reveals the real impact that one dynamics has on the other much more reliably than the coupling strength.

We choose the variance as a data-driven estimator of the dynamics' energy because it is a simple and intuitive quantity. Our results show that it is well-suited to address symmetric interactions in non-identical coupled dynamics. On the other hand, we still at times have a remaining mismatch. In some cases equal estimates of interaction in both directions are obtained for only approximately equal coupling impact values. Hence, an open topic for a future study is to test higher order moments for the esti-

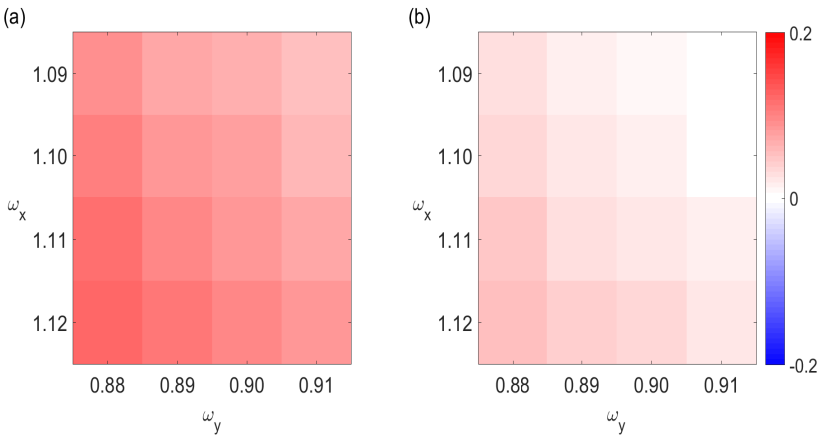

Figure 4.10: The coupling impact correctly detects symmetric interactions for the noisy van der Pol oscillators. Values of ρ_ϵ (a) and ρ_γ (b) for different frequency levels. We vary the frequencies $\omega_{x,y}$ while the noise levels $\xi_{x,y}$ are fixed to 0.04.

mation of the dynamics' energy. Furthermore, we can consider dynamics that are coupled not only diffusively but which have more complex interactions.

It is important to underline the scope of this work. For real-world data one does not know in general the values of the coupling strength of the underlying dynamics. Furthermore, the variance of real-world signals might not reflect well the true energy that one dynamics exerts on the other, but instead depends on the measurement. An important aspect is the path between the place where the dynamics takes place and the location of the measurement device. In electroencephalographic recordings, for example, the activity of the interacting neurons takes place in the brain but electrodes are placed on different positions of the scalp. More-

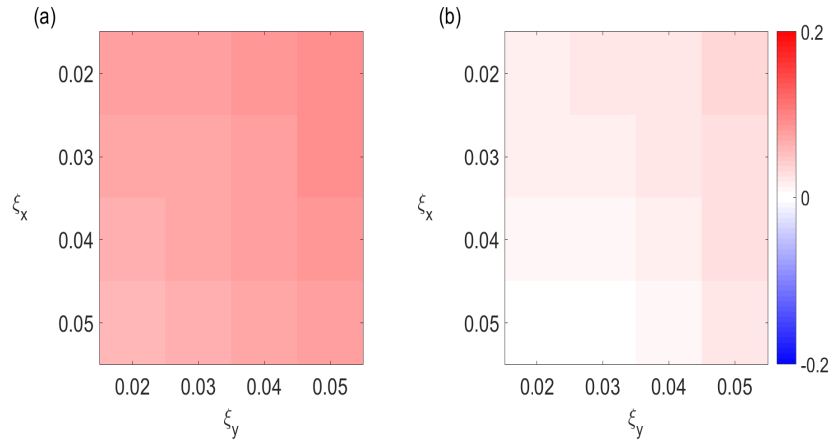

Figure 4.11: Same as Fig. 4.10 but for different noise levels. The frequencies ω_x, ω_y are fixed to 1.1 and 0.9 respectively and the noise levels $\xi_{x,y}$ vary.

over, the electrode impedance is not identical across different electrodes. Hence, the variance of electroencephalographic recordings cannot be the real variance of the signal through which the coupling is conveyed. For these reasons an application of the coupling impact to experimental data is not straightforward.

We also note that noisy dynamics with time-varying parameters can be analyzed with the dynamical Bayesian inference approach [67, 68, 17, 57] that reveals the effective connectivity. However, the phase-based approach that we applied here as well as the dynamical Bayesian inference approach are model-based [52] while the state space approach does not assume any model of the interacting dynamics.

Concluding, we underline that the aim of this study is not to propose the coupling impact as a measure to analyze experimental data. Instead, it serves as a way to define symmetric interactions between bidirection-

ally coupled dynamics, regardless of whether or not they are identical. Therefore, although we follow a data-driven approach our contribution is towards an understanding of dynamical systems.

Chapter 5

INTERACTIONS BETWEEN TWO ENSEMBLES OF COUPLED DYNAMICS

5.1 Introduction

From interactions between two individual dynamics we now move to interactions between two ensembles of dynamics. In nature there are many dynamics with collective behaviour. The measurements of such dynamics are at a macroscopic instead at a microscopic level. In other words the measurements of real-world dynamics often reflect the average activity of the individual units of the dynamics. This average activity is expressed through the mean field signal. A characteristic example is the brain where the electroencephalographic recording indicates the average electrical activity of groups of neurons [13]. Apart from the real-world dynamics there are many model systems with collective behavior. Such systems consist of ensembles of dynamics that are coupled via many ways like global the so-called all to all and random coupling. The mean fields of the ensembles usually act as variables of the system through which the individual dynamics of the same or different ensembles interact [48, 47]. There are studies where a quantitative analysis of the mean field signals

aims at the characterization of synchronization between the individual dynamics of the ensembles [49, 63]. Moreover, Cimponeriu et. al. [16] applied a phase-based approach to the mean fields of two coupled neuronal ensembles in order to characterize directional interactions between them. In this study, we apply the state-space measure L to the mean fields of two coupled ensembles of chaotic dynamics. We consider cases where the individual dynamics of the ensembles are globally coupled and uncoupled. We investigate the role of different parameters for the detection of interaction between the two populations such as the population size and the data length of the signals. Moreover, we use different types of chaotic dynamics and we test the accuracy of the measure L when measurement noise is present. In the end, we show the advantage of L over its previous version the so-called measure M (Sec. 3.2.2).

5.2 Methods

The model systems that we analyze consist of two ensembles of chaotic dynamics, A and B (Fig. 5.1). Each ensemble contains P dynamics that are weakly globally coupled with intracoupling strength μ. Furthermore, each dynamics of the A ensemble is unidirectionally coupled with exactly one dynamics of the B ensemble, with intercoupling strength ν. The A and B ensembles both consist of non-identical Rössler or Lorenz dynamics. The A ensemble of the Rössler dynamics [49] is described by:

$$\begin{aligned}
\dot{x}_\lambda(t) &= -\omega_\lambda\, y_\lambda(t) - z_\lambda(t) + \mu(X(t) - x_\lambda(t)),\\
\dot{y}_\lambda(t) &= \omega_\lambda\, x_\lambda(t) + 0.25\, y_\lambda(t),\\
\dot{z}_\lambda(t) &= (x_\lambda(t) - 8.5)\, z_\lambda(t) + 0.4,
\end{aligned} \tag{5.1}$$

while the B ensemble reads:

$$\begin{aligned}
\dot{u}_\lambda(t) &= -\omega_\lambda\, v_\lambda(t) - w_\lambda(t) + \mu(Y(t) - u_\lambda(t)) + \nu\,(x_\lambda(t) - u_\lambda(t)),\\
\dot{v}_\lambda(t) &= \omega_\lambda\, u_\lambda(t) + 0.25\, v_\lambda(t),\\
\dot{w}_\lambda(t) &= (u_\lambda(t) - 8.5)\, w_\lambda(t) + 0.4,
\end{aligned} \tag{5.2}$$

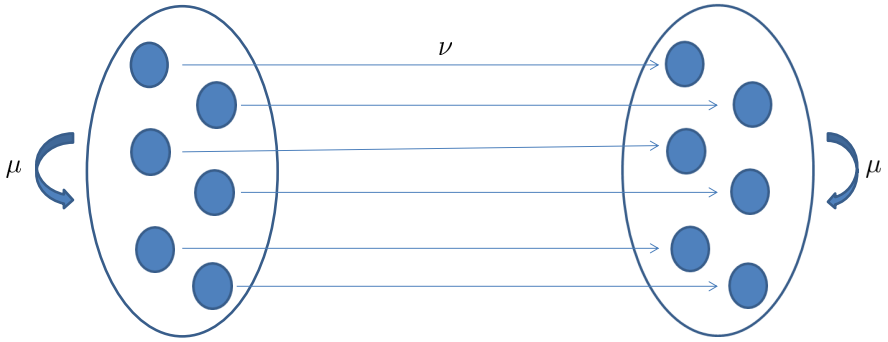

Figure 5.1: The coupling scheme between the A (left) and B (right) ensembles.

where $\lambda = 1, \ldots, P$. The variables $X = 1/P \sum_{\lambda=1}^{P} x_\lambda$ and $Y = 1/P \sum_{\lambda=1}^{P} u_\lambda$ stand for the mean field of the A and B ensemble, respectively. The parameters ω_λ denote the frequencies of the individual Rössler dynamics and they are randomly selected from a uniform distribution $U(a, b)$. For the A ensemble $\omega_\lambda \sim U(0.93, 0.97)$, while for the B ensemble $\omega_\lambda \sim U(0.96, 1)$. The intercoupling values ν run from 0 to 0.17 in steps of 0.0189. The intracoupling value μ is fixed to either $\mu = 0$ or $\mu = 0.02$. We use the fourth order Runge-Kutta method to numerically integrate these dynamics with step size of 0.05 time units and sampling interval of $\Delta t = 0.6$ time units. In every cycle of the dynamics correspond 12 points, approximately.

Regarding the Lorenz dynamics, the A ensemble is described by:

$$
\begin{aligned}
\dot{x}_\lambda(t) &= 10\,(-x_\lambda(t) + y_\lambda(t)) + \mu\,(X(t) - x_\lambda(t)),\\
\dot{y}_\lambda(t) &= R_\lambda\, x_\lambda(t) - y_\lambda(t) - x_\lambda(t)\, z_\lambda(t),\\
\dot{z}_\lambda(t) &= x_\lambda(t)\, y_\lambda(t) - \frac{8}{3}\, z_\lambda(t),
\end{aligned}
\tag{5.3}
$$

and the B ensemble reads:

$$
\begin{aligned}
\dot{u}_\lambda(t) &= 10\,(-u_\lambda(t) + v_\lambda(t)) + \mu\,(Y(t) - u_\lambda(t)) + \nu\,(x_\lambda(t) - u_\lambda(t)),\\
\dot{v}_\lambda(t) &= R_\lambda\, u_\lambda(t) - v_\lambda(t) - u_\lambda(t)\, w_\lambda(t),\\
\dot{w}_\lambda(t) &= u_\lambda(t)\, v_\lambda(t) - \frac{8}{3}\, w_\lambda(t).
\end{aligned}
\tag{5.4}
$$

In analogy to the definitions of the Rössler dynamics $\lambda = 1, \ldots, P$ and the variables $X = 1/P \sum_{\lambda=1}^{P} x_\lambda$ and $Y = 1/P \sum_{\lambda=1}^{P} u_\lambda$ indicate the mean field of the A and B ensemble, respectively. The parameters R_λ are randomly selected from a uniform distribution. Particularly, $R_\lambda \sim U(37, 39)$ for the A ensemble and $R_\lambda \sim U(43, 45)$ for the B ensemble. Here, the ν values run from 0 to 8 in steps of 1, while μ is fixed to either $\mu = 0$ or $\mu = 0.5$. For the numerical integration we use the fourth order Runge-Kutta method with step size of 0.005 time units and sampling interval of $\Delta t = 0.06$ time units. Again, every cycle consists of 12 points, approximately. We underline that for all the dynamics we always use random initial conditions and we apply preiterations in the numerical integration to discard transients.

In our analysis the intercoupling values ν vary while the intracoupling value μ is fixed. We consider two cases for the μ value. In the first case, $\mu = 0$, which implies that the dynamics within the same ensemble are uncoupled. In the second one, μ takes a non-zero value and the dynamics within the same ensemble are weakly globally coupled. When the dynamics of the same ensemble are coupled many phenomena can occur like partial [46] and intermittent synchrony [70]. In our study, the selection of μ and ν coupling values is done such that the dynamics which belong to the same or different ensembles do not have a synchronous motion. For each intercoupling value ν we obtain from the A and B ensembles the X and Y mean fields respectively and we apply to them the

measure $\Delta L = L(X|Y) - L(Y|X)$. We repeat this process for 20 independent realizations and afterwards we calculate the mean values of $\langle \Delta L \rangle$. Moreover, for the implementation of the measure L we use the same parameters like our previous study (Sec. 4.2.2). In our analysis we examine the effect of different parameters in the detection of coupling by the measure L. We test the role of the population size P by considering different sizes ($P = 2, 50, 500, 5000$). We also examine the effect of the data length of the mean field signals. In particular, we use signals which consist of $N = 300, 1000, 3000$ and 6000 data points and we investigate the influence of observational noise. In addition, we test the effect of the number of interlinks between the individual dynamics of the two ensembles on the detection of coupling.

Before we show the results of the analysis it is important to have a visual inspection of the signals. We illustrate the mean field signal X of the Rössler ensemble (Eqs. (5.1)) for intracoupling value $\mu = 0$ and for different ensemble size P (Fig. 5.2). We observe that as the size of the ensemble is increasing, the amplitude of the mean field X is decreasing. This is more evident on Fig. 5.3 where we depict the standard deviation s_A of the mean field X for different P values.

5.3 Results

We divide our analysis into parts. In the firt part we use the Rössler ensembles (Eqs. (5.1)-(5.2)) and in the second one we use the Lorenz ensembles (Eqs. (5.3)-(5.4)).

5.3.1 Rössler ensembles

We start to present the results by illustrating the values of the measure L for different ensemble sizes P and for different data lengths of the signals. We use the Rössler ensembles with intracoupling strength $\mu = 0$. Fig. 5.4 demonstrates that L is sensitive enough to capture the intercoupling strength ν (coupling from the A ensemble to the B ensemble)

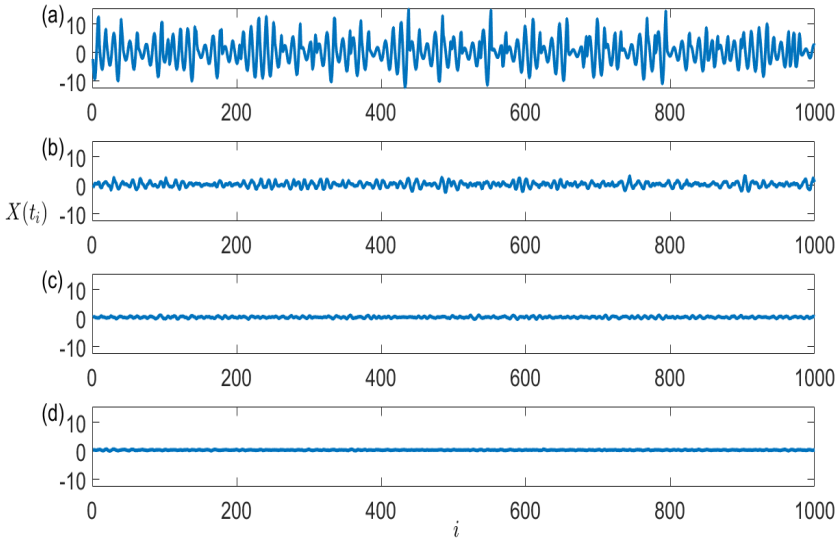

Figure 5.2: The amplitude of the mean field signal is decreasing as the population size is increasing. Mean field signals $X(t_i), i = 1, \ldots, 1000$ of the Rössler ensembles (Eqs. (5.1)) for intracoupling strength $\mu = 0$ and different ensemble size P ($P = 2$ (a) , $P = 50$ (b), $P = 500$ (c) and $P = 5000$ (d)).

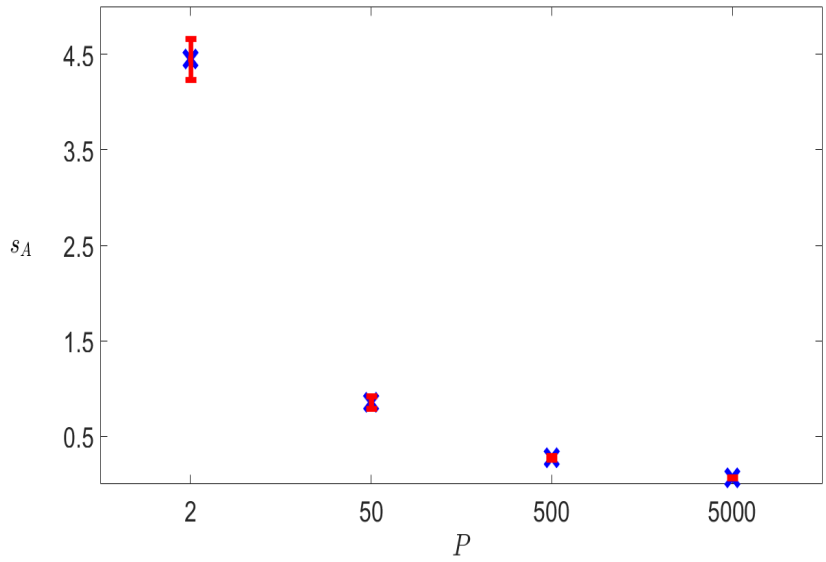

Figure 5.3: The standard deviation of the mean field signal is decreasing with the increase of the ensemble size P. Mean values of the standard deviation of the mean field X for the Rössler ensemble of Fig. 5.2. The errorbars illustrate the mean $\pm$ one standard deviation across 20 independent realizations.

when it is present. In general, as the values of ν are increasing the values of $L(X|Y)$ (blue line) also increase. However, we also observe an increase in the values of $L(Y|X)$ (green line), despite the fact that there is no coupling from the B ensemble to the A ensemble. This behavior is not peculiar but reflects the characteristics of the state similarity criterion (Sec. 3.2.1). In general, in unidirectionally coupled dynamics the state-space measures detect the coupling not only in the direction where it is really present, but also in the other direction that is absent [15]. However, the detection of the coupling in the latter case holds to a weaker degree. Hence, in order to find the predominant direction of coupling between two interacting dynamics we should always consider the difference of the measure L in both directions [15].

In our analysis we say that the measure L is able to detect a positive intercoupling value ν if across the 20 independent realizations the values of $\Delta L = L(X|Y) - L(Y|X)$ are significantly positive as assessed by a Wilcoxon rank sum test. Our analysis requires many levels of multiple testing. Apart from the 8 non-zero coupling values, we have 4 different data length of the signals and 4 different population sizes. Therefore, due to the Bonferoni correction [62], we set the significance level to $\alpha = 0.05/128 = 3.9 \times 10^{-4}$. Fig. 5.4 shows that as the data length of the mean fields is increasing the measure L gets more sensitive and captures small intercoupling values ν. On the other hand, as the ensemble size is increasing the values of L decrease and the difference ΔL gets smaller. However, it still remains significant. We can also see a clear difference between the top-left panel and bottom-right panel. Although, on the top-left panel the differences between the L values are large however, due to their large variability they are not significant. On the contrary, the small variability of the L values in the bottom-right panel render them significant despite their small difference.

We quantify the performance Ψ of the measure L by calculating the fraction of the number of the non-zero intercoupling values ν for which we have significant detection of coupling over the total number n_ν of the non-zero intercoupling values. Hence, the Ψ values vary from 0 (com-

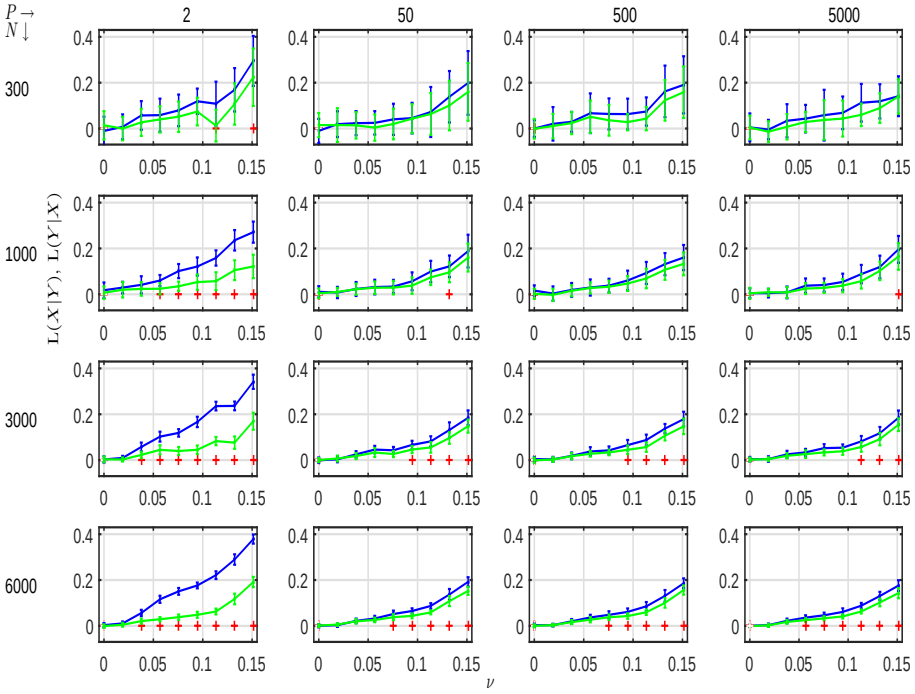

Figure 5.4: The measure L is able to detect the coupling between ensembles of dynamics from their mean fields. Values of $L(X|Y)$ (blue) and $L(Y|X)$ (green) for the Rössler ensembles (Eqs. (5.1)-(5.2)) with $\mu = 0$. The error bars depict the mean $\pm$ one standard deviation across 20 independent realizations. Red crosses label the intercoupling values ν for which we have significant detection of coupling. From one column to the other the population size P is increasing. From top to bottom the data length N of the mean field signals is increasing.

plete failure of detection of non-zero intercoupling values) to 1 (successful detection of all the non-zero intercoupling values). Fig. 5.5 depicts the performance of the measure L for $\mu = 0$ (a) and $\mu = 0.02$ (b). We see that when the dynamics within the same ensemble are weakly globally coupled the performance of the measure L gets better. Moreover, for both intracoupling values μ the increase of the lengths of the mean

field signals boosts the Ψ values. Obviously, this does not hold with the increase of the population size P. In the analysis that we did for Fig.

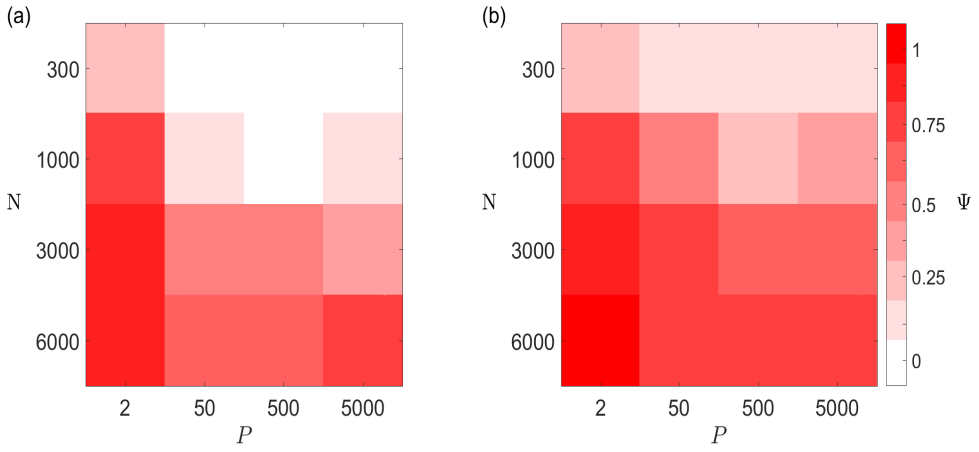

Figure 5.5: The performance of the measure L gets better with the presence of intracoupling strength. Ψ values of the Rössler ensembles for intracoupling strength $\mu = 0$ (a) and $\mu = 0.02$ (b).

5.5 we examined the sensitivity of the measure L. It is also important to test its specificity (i.e. detection of the absence of coupling). Thus, we create one more auxiliary system of Rössler ensembles, A' and B'. The auxiliary system has the same parameters with the one of the A and B ensembles (Eqs. (5.1)-(5.2)) but for its generation we use different initial conditions. For the analysis we use the mean field signal X of the A ensemble and the mean field signal Y not from the B ensemble but from the B'. Since the A, B ensembles are independent from the A', B' ensembles there is no presence of coupling between the A and B' ensembles. Fig. 5.6 shows that indeed the measure L does not detect the presence of any coupling between the A and B' ensembles since all the Ψ values are zero.

This holds when the dynamics within the same ensemble are uncoupled as well as when they are weakly globally coupled.

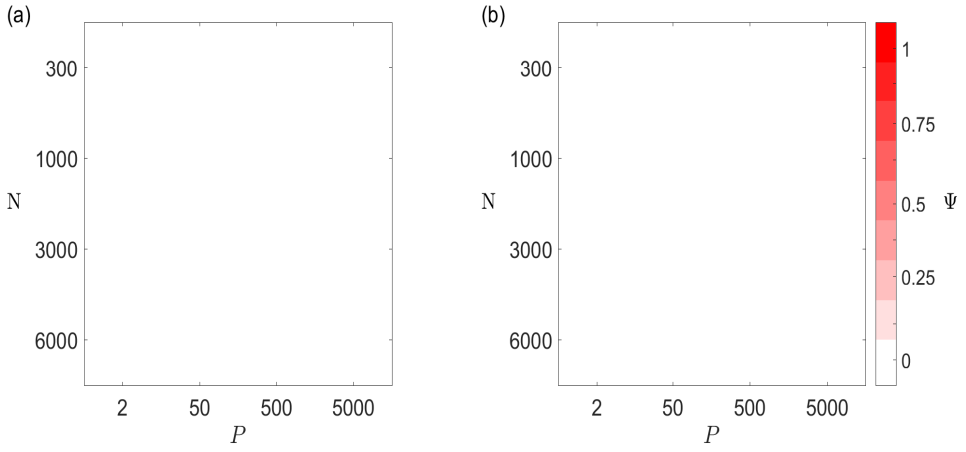

Figure 5.6: The measure L correctly detects the absence of coupling between two independent ensembles. Performance of L for the independent Rössler ensembles A and B'. In (a) the intracoupling strength is $\mu = 0$ while in (b) it is $\mu = 0.02$.

In order to evaluate the accuracy of the results of Fig. 5.5 we apply the following process. For each intercoupling value ν, we make 60 independent realizations and we split them in three groups each of which contains 20 realizations. For each group we calculate the performance Ψ of L and afterwards we estimate the mean and range of the Ψ values across the three groups (Fig. 5.7). We observe that the range is either zero or it deviates at most 2 coupling values from the mean. Therefore, the results of Fig. 5.5 are accurate.

So far, we evaluated the performance of the measure L for different lengths of the mean field signals as well as for different ensemble sizes.

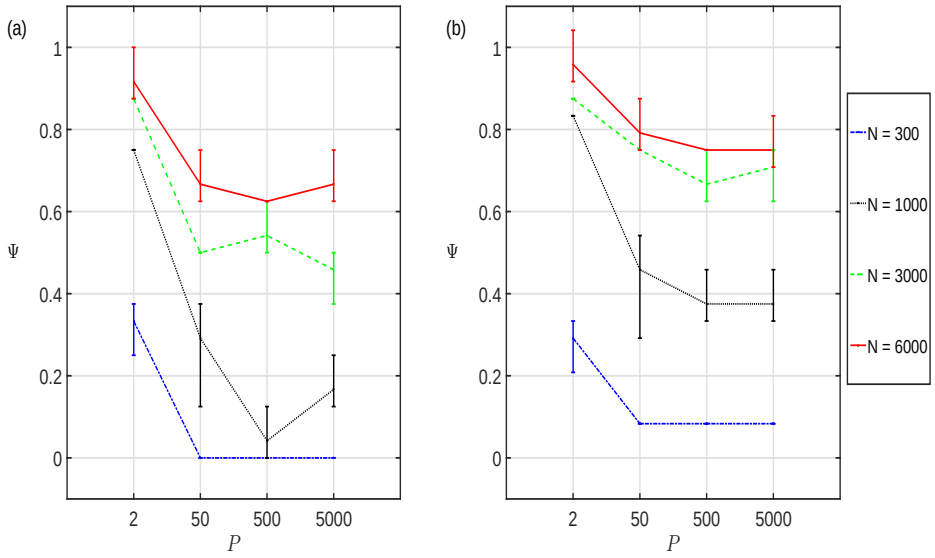

Figure 5.7: Accuracy of the results of Fig. 5.5. Mean values of the performance Ψ obtained across 3 sets of 20 independent realizations each. In (a) $\mu = 0$ while in (b) $\mu = 0.02$. Error bars depict the corresponding ranges.

We saw that when the data length is small the directional coupling between the two ensembles is hardly detectable by the measure L (Fig. 5.4). However, as long as the signals have enough data, L correctly detects the coupling even for large ensemble sizes. Therefore, it is essential to find the limit of the ensemble size P for which L does not detect the coupling between the two populations. From our study we found that even for very large ensembles (P was in the order of 10^5) L was able to capture the directional coupling between the two ensembles. Moreover, we observed a stability in the values of L, which is already visible in Fig. 5.4. On the last three columns and for enough data length ($N = 3000, 6000$) we observe that although the ensemble sizes are different the values of L show a similarity across the different panels.

The fact that the measure L correctly detects the presence and ab-

sence of coupling even for very large ensembles means that the mean fields X and Y carry the information of the individual dynamics. Hence, we have to study the mechanism under which the information is transferred from the individual dynamics x_j, $j = 1, \ldots, P$ to the mean field $X = 1/N \sum_{i=j}^{P} x_j$. In other words, we have to find what common has the mean field with the individual dynamics of the population.

We consider Rössler ensembles A and B with size P that ranges from 2 to 19000 in various steps. We fix the intracoupling value $\mu = 0$ and the intercoupling value $\nu = 0.1512$. From the A and B ensembles we obtain the mean field signals X and Y and apply to them the measure ΔL. Moreover, we calculate their corresponding standard deviations s_A, s_B, respectively. As an order parameter e.g. for the A ensemble, we use the quantity $\rho_A = \mathrm{rms}(X)/\langle \mathrm{rms}(x_j) \rangle$(see also [18]), where rms stands for the root mean square error. From Fig. 5.8(a) we observe that the difference ΔL gradually decreases with the increase of the P values. However, the ΔL values tend to become stable for $P > 10$. Panels (b),(c) also demonstrate that with the increase of the ensemble size the standard deviation s_A as well as the order parameter ρ_A decrease.

Now we will study the mechanism under which the information is transferred from the individual dynamics to the mean fields. In particular, we will use the embedding vectors of the signals since the measure L is based on the state space reconstruction via embedding vectors (Sec. 3.2.2). Let us assume that we take the signal of the x_j $j = 1, \ldots, P$ dynamics of the ensemble with length $i = 1, \ldots, N$. With $\mathbf{x}_a$, $a = (m-1)\tau + 1, \ldots, N$ we denote its embedding vectors. Moreover, $\mathbf{z}_a$ stands for the embedding vectors of the mean field signal X. We indicate with $\boldsymbol{\beta}_a$ and $\boldsymbol{\delta}_a$ the vectors whose elements are the time indexes of all the k spatial close neighbors of $\mathbf{x}_a$ and $\mathbf{z}_a$, respectively. We count the total number of a values for which $\{\boldsymbol{\beta}_a \cap \boldsymbol{\delta}_a \neq \emptyset\}$ and we denote this number with c_j. In other words, c_j indicates the number of embedding vectors for which the mean field and the j-th dynamics have at least one spatial close neighbor with the same time index,

$$c_j = \left| \bigcup_a \{\boldsymbol{\beta}_a \cap \boldsymbol{\delta}_a \neq \emptyset\} \right|. \tag{5.5}$$

We estimate the c_j values for each j dynamics of the ensemble and afterwards, we calculate the average value $c_A = \langle c_j \rangle, j = 1, \ldots, P$. Fig. 5.8(d) illustrates the c_A values for different ensemble size P. We observe that as the ensemble size is increasing, the c_A values gradually decrease. However, they become stable for $P > 1000$. We also observe that panel (d) has a relation with panel (a). The higher the c_A values are, the greater ΔL values we get. When the c_A values start to become stable, we also have a stability in the ΔL values. In other words, when the c_A values become stable the information that is transferred from the individual dynamics to the mean field saturates and this is reflected by the similarity of the ΔL values. We underline that if we calculate the average cardinality of the set $\{\boldsymbol{\beta}_a \cap \boldsymbol{\delta}_a \neq \emptyset\}$ across all the a values we obtain similar results like Fig. 5.8(d) with an upper and lower limit of 1.1 and 1, respectively.

We now test the robustness of L against noise. For this, we contaminate the mean field signals with observational Gaussian noise with zero mean and standard deviation ξ percent of the standard deviation of the mean field. The values of ξ are $\xi = 10, 30, 50$ and 100. Fig. 5.9 shows that as the percentage of the noise level is increasing the performance Ψ of the measure L is decreasing. The presence of the intracoupling strength μ increases the Ψ values. On the other hand, the increase of the ensemble size reduces the performance of L regardless of the presence of the intracoupling.

In our analysis, we also investigate the effect of the number of interlinks (connections between the individual dynamics of the A to the B ensemble) on the detection of the coupling between the two Rössler ensembles. We know that each dynamics of the A ensemble is unidirectionally coupled with exactly one dynamics of the B ensemble. We start removing these interlinks and we test the performance of the measure L in such cases. Here, the ensemble size takes values $P = 50, 100, 500$ and 5000. Moreover, the percentage of interlinks ζ that are present between the individual dynamics of the ensembles is ζ percent of the population size P, where $\zeta = 35, 65, 85$ and 95. Fig. 5.10 (a) shows that when the intracoupling value $\mu = 0$, L does not detect the presence of coupling between the two ensembles for $\zeta \leq 65$. As we increase the percentage

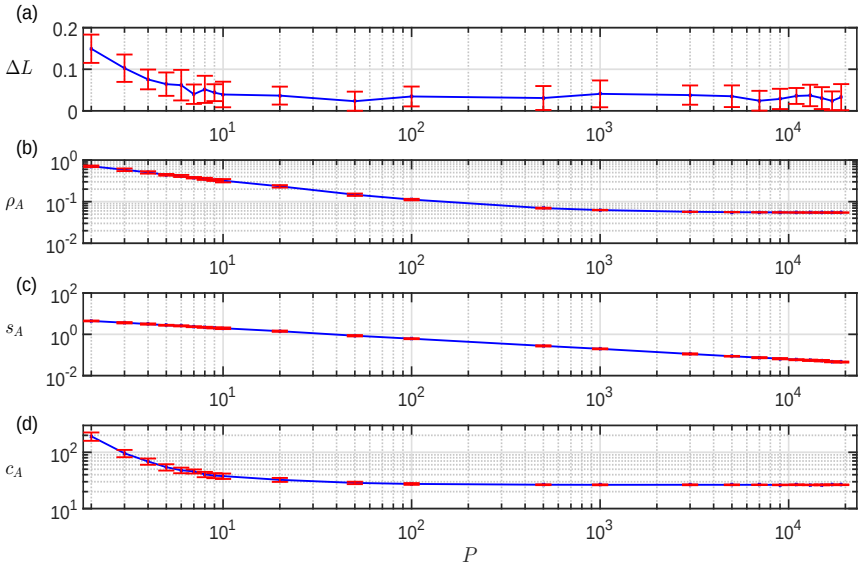

Figure 5.8: Analogy between the ΔL and c_P values. Panel (a) illustrates the mean values of ΔL of the Rössler ensembles (Eqs. (5.1)-(5.2)) for $\mu = 0$. Panels (b)-(d) correspond to the A ensemble. They depict mean values of the order parameter of the population A (b), the standard deviation of the mean field X and the c_A values (c). Error bars show the mean $\pm$ one standard deviation across 20 independent realizations. The length of the signals is $N = 1000$ data points.

of the interlinks between the dynamics of the two populations, we have better performance of the measure L. This result is reasonable since by removing the interlinks between the two ensembles the two mean fields become more independent. By adding interlinks, the mean fields become more dependent and this results to an increase of the performance of L. Moreover, the presence of intracoupling (Fig. 5.10 (b)) is beneficial again since it increases the performance of L. Regarding the increase of the ensemble size we cannot say that in this case it reduces the performance of L since we observe in general similar Ψ values across the difference ensemble sizes.

We close the analysis of the Rössler ensembles by evaluating the per-

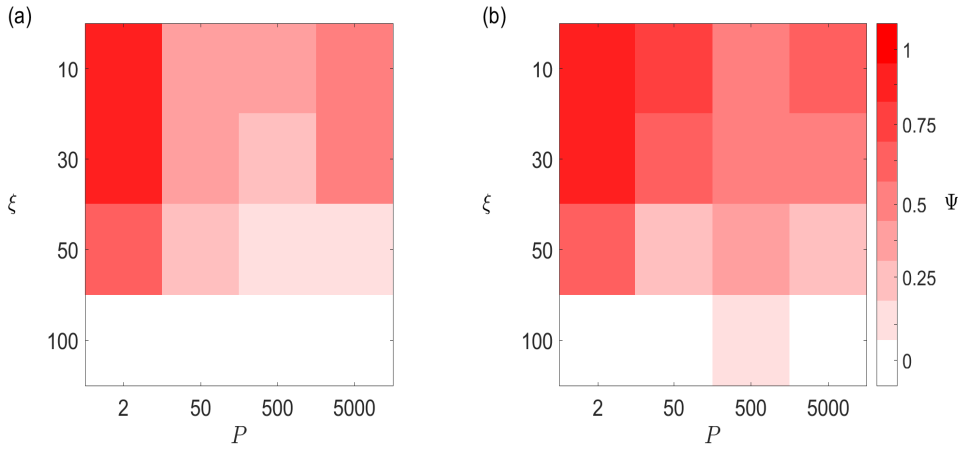

Figure 5.9: The measure L captures the coupling from noisy mean field signals. Performance of the measure L for different noise levels ξ and for different ensemble sizes P. In (a) $\mu = 0$ and in (b) $\mu = 0.02$. The length of the mean field signals is $N = 3000$.

formance of the measure L over its previous version, the measure M [4] (Sec. 3.2.2). Chicharro and Andrzejak [15] showed that in unidirectionally coupled dynamics L has better sensitivity and specificity than M. Here, we illustrate the difference $\Delta\Psi = \Psi(L) - \Psi(M)$ between the performances of L and M denoted by $\Psi(L)$ and $\Psi(M)$, respectively. Positive values of $\Delta\Psi$ with an upper limit of 1 imply that L performs better than M, while the contrary is indicated by negative values of $\Delta\Psi$ and a lower limit of -1. Zero values of $\Delta\Psi$ imply equal performance of the measures. The panels of Fig. 5.11 are in analogy with Figs. 5.5, 5.9, 5.10 but they depict the difference $\Delta\Psi$. We see that in general L prevails over M, but sometimes they have the same performance.

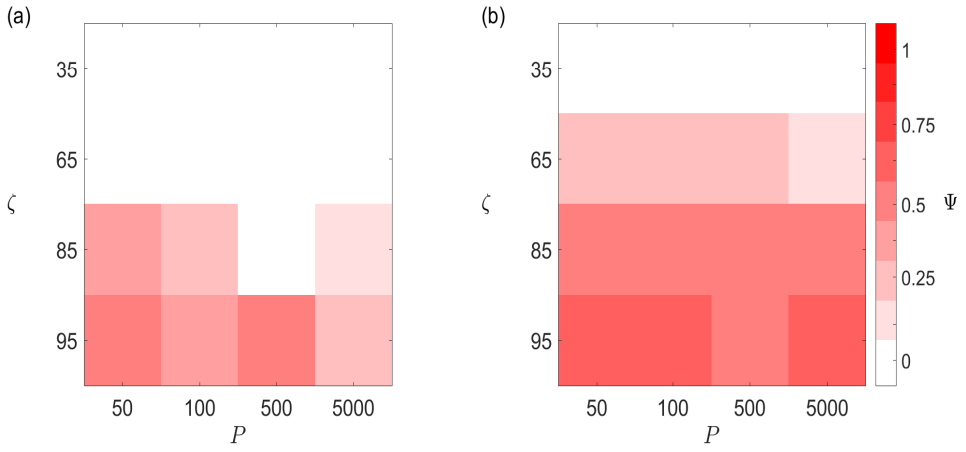

Figure 5.10: The performance of L is decreasing as the number of interlinks between the dynamics of the two ensembles are decreasing. Ψ values for different percentages of interlinks between the Rössler ensembles. In (a) $\mu = 0$ and in (b) $\mu = 0.02$. The length of the mean field signals is $N = 3000$.

5.3.2 Lorenz ensembles

Regarding the Lorenz ensembles the results are similar with the Rössler ensembles. Fig. 5.12 illustrates the Ψ values for various ensemble sizes and lengths of the mean field signals. We observe that the large data length improves the performance of L. Moreover, the increase of the ensemble size reduces the values of $\Delta L = L(X|Y) - L(Y|X)$, but they still remain significant for long enough signals. Figs. 5.13-5.15 are in analogy with Figs. 5.5, 5.9, 5.10 of the Rössler ensembles. We see that the performance of L is better in the Rössler dynamics particularly for the signals with small data length and for those which are contaminated with noise. However, in Lorenz ensembles L captures the coupling between the two ensembles even with small number of interlinks. Concerning the

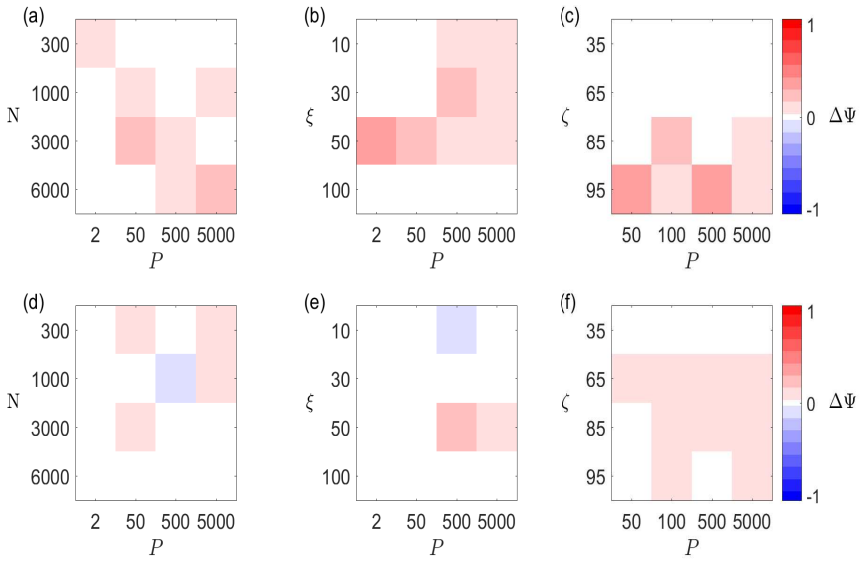

Figure 5.11: L is in general more sensitive than M since it can better capture the coupling between the two ensembles. The panels of each column correspond to Figs. 5.5, 5.9, 5.10 respectively but they illustrate the difference $\Delta\Psi$ between the performances of L and M. In the first row the intracoupling is zero while in the second one it is positive.

advantage of L over M, Fig. 5.16 clearly demonstrates that L prevails over M. Here the advantage of L over M is more evident than in the Rössler ensembles.

5.4 Discussion

In this study we wanted to examine if we can detect directional couplings between pairs of ensembles of coupled dynamics from the mean fields. We followed a data-driven approach by applying the measure L to the mean field signals of the ensembles. We evaluated the sensitivity and specificity of L by investigating the role of different parameters such as

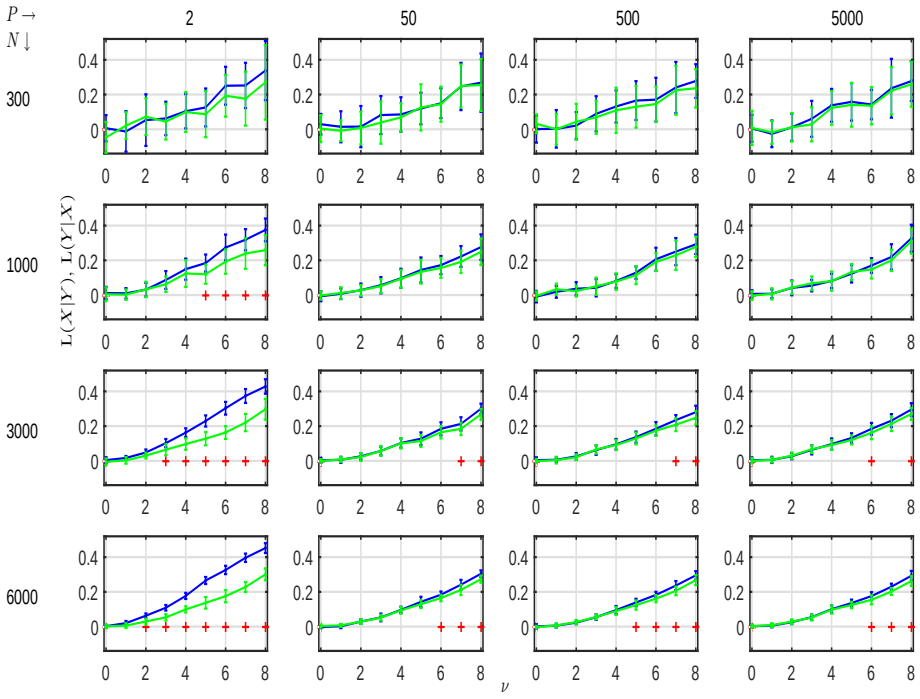

Figure 5.12: Same as Fig. 5.4 but for the Lorenz ensembles.

the population size and the length of the signals. Moreover, we used different types of chaotic dynamics (Rössler and Lorenz) and we tested the accuracy of the measure L when measurement noise is present. Additionally, we tested the effect of the number of interlinks between the dynamics of the ensembles on the detection of coupling.

We found that L successfully captures directional couplings from the mean fields of the coupled ensembles. Particularly, we showed that signals with long data as well as the presence of weak intracoupling boost the sensitivity of L (Fig. 5.5). However, the performance of L is reduced with the increase of the ensemble size. Here, we observed a phenomenon where for large ensembles L was not only able to capture directional cou-

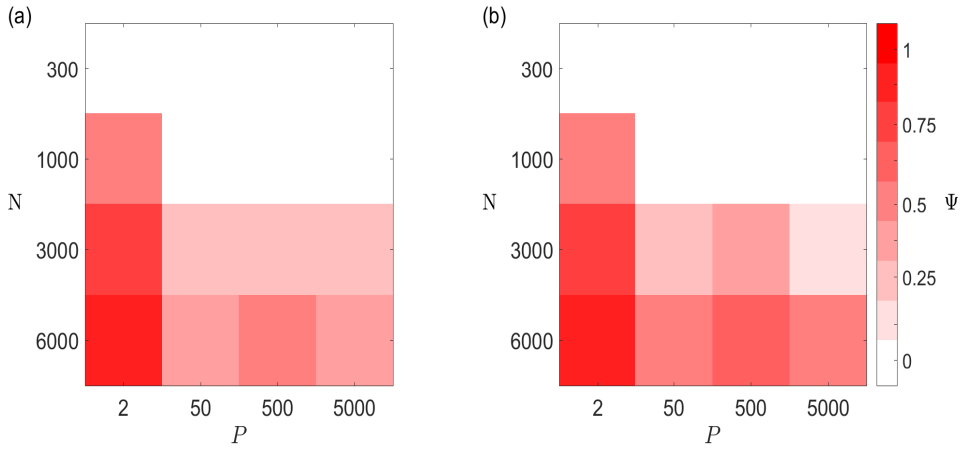

Figure 5.13: Same as Fig. 5.5 but for the Lorenz ensembles.

plings between the mean fields of the two populations, but it also took similar values across different ensemble sizes. We showed that the reason for this behavior is that the information which is transferred from the individual dynamics to the mean filed saturates (Fig. 5.8). This saturation is expressed via the embedding vectors in the sense that across different population sizes the average number of embedding vectors for which the mean field and the individual dynamics have at least one common neighbor is the same. Furthermore, we showed that the measure L is robust to observational noise (Fig. 5.9) and in general it is more sensitive than its previous version the so-called measure M (Fig. 5.16). We observed these results not only for the Rössler ensembles but also for Lorenz ensembles.

We have to mention that for the intercoupling values ν for which we had significant detection of coupling, the difference ΔL between the L values in both directions was small. Small but significant ΔL values are often met in the analysis of biomedical data. On the contrary, when L is

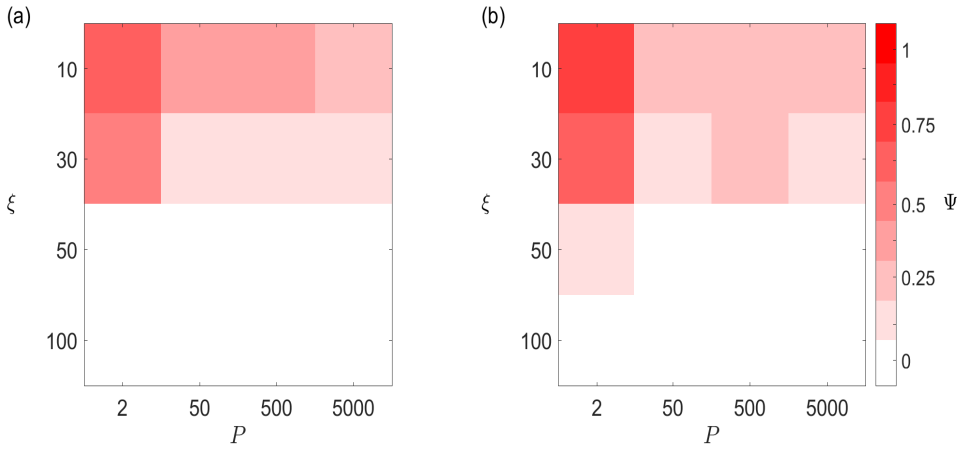

Figure 5.14: Same as Fig. 5.9 but for the Lorenz ensembles.

applied to model uni- [15] or bidirectionally [33] coupled dynamics ΔL gets higher values.

Summarizing we can say that our study provides good indications that the measure L is able to detect directional couplings between ensembles of dynamics from their mean fields. We underline that the signals which are used for the analysis should have enough data. Future studies can consider applications of the measure L to neuronal models since these types of models better simulate real-world dynamics. Moreover, different types and ways of coupling can be considered. Here, the dynamics which belong to the same ensemble were globally coupled whereas the coupling between the dynamics of different ensembles was one to one. It would be interesting to test another types of coupling such as non-local and random coupling. Moreover, it would be interesting to study networks of interacting ensembles and evaluate the performance of L.

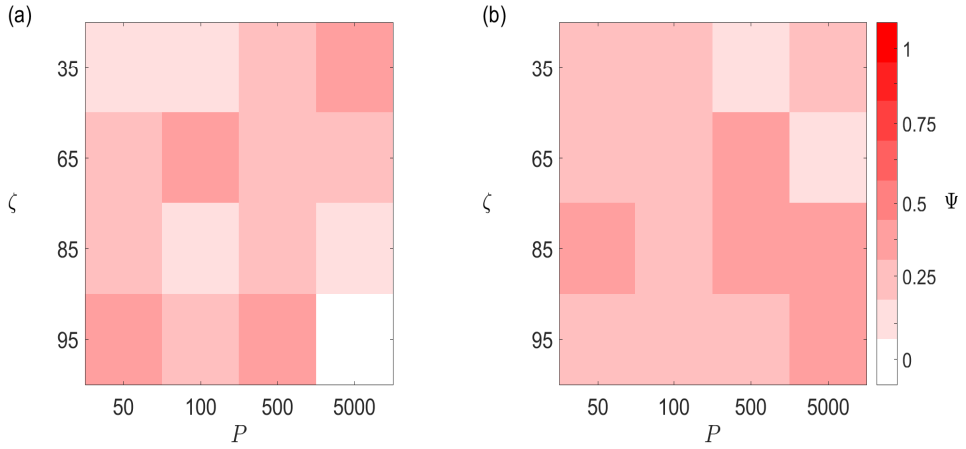

Figure 5.15: Same as Fig. 5.10 but for the Lorenz ensembles.

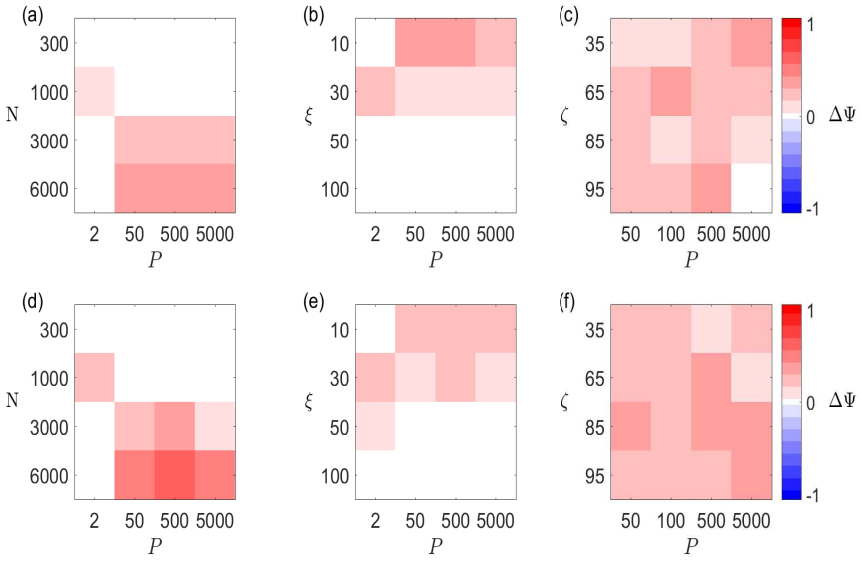

Figure 5.16: Same as Fig. 5.11 but for the Lorenz ensembles.

Chapter 6

CONCLUSIONS

In this thesis we followed a data-driven analysis in order to characterize interactions between coupled dynamics. We used two approaches with different modalities and characteristics, the state-space measure L [15] and the phase-based measure d [54, 27, 28]. It has already been demonstrated that these approaches correctly detect directional interactions in simple unidirectionally coupled model dynamics. With this study we wanted to investigate directional interactions in more complex dynamics. Questions that motivated our research include: Can we characterize interactions in pairs of non-identical bidirectionally coupled dynamics? Is it possible to detect directional couplings from ensembles of dynamics?

In the beginning of this thesis we provided the theoretical concept about dynamical systems (Ch. 2) and explained the algorithms of the data-driven approaches (Ch. 3). Afterwards, we analyzed pairs of bidirectionally coupled dynamics (Ch. 4). We characterized directional interactions in pairs of bidirectionally coupled dynamics. In particular, we introduced the notion of the coupling impact that more accurate reveals the real effect that one dynamics has on the other. We showed that the coupling impact, in contrast to the coupling strength varies monotonically with the values of data-driven approaches.

Subsequently, we analyzed high dimentional dynamics. We investigated directional interactions between pairs of ensembles of coupled dy-

namics (Ch. 5). Here, we only used the state-space approach L since the variation of the mean-field signals did not allow us to obtain well-defined phases. We showed that we are able to detect not only the strength but also the direction of the coupling even for interactions which occur between large ensembles. Detailed conclusions about the results of each study on pairs and ensembles of coupled dynamics are given in the end of Ch. 4 and 5, respectively.

The dynamics that we used in our study were model dynamics. Concerning the applications of the measure L and d to real-world experimental data one should always take into account the characteristics of the signals and the assumptions of the approaches. Directional couplings can be only inferred in weakly coupled dynamics which are not yet synchronized. When the interacting dynamics are strongly coupled they form a unit and the detection of the direction is no longer possible. Moreover, the phase-based measure requires well-defined phases. On the other hand, the state-space measure L requires the dynamics to be aperiodic. To calculate these measures many parameters have to be fixed (Ch. 3). The best selection of these parameters is based on the fact that we always have to test different ranges and select the ones for which the corresponding measure has stable results. Additionally, for real-world applications one can consider the use of surrogate data [61]. Surrogate data are constrained randomizations of the original data that share specific properties with them. A hypothesis test is performed and the null hypothesis is composed with assumptions that we want to test (e.g. linear stochastic Gaussian process). Previous studies demonstrated that the use of surrogate can be powerful if we want to test non-linear dependences, between coupled dynamics aas well as stationarity and randomness of individual dynamics [7, 55, 6].

The results of our study demonstrate that directional couplings between complex dynamics can be inferred from an analysis of their signals. In particular we achived to characterize interactions between pairs of non-identical bidirectionally coupled dynamics. We introduced the notion of the coupling impact which better reflects the real effect that one dynamics has on the other for different degrees of their asymmetry [33]. Moreover, we demonstrated that we are able to detect the strength and the direc-

tion of interaction in large ensembles of coupled dynamics. The different data-driven approaches L and d successfully captured the directional couplings of the dynamics. In particular, the measure L demonstrated very good accuracy not only in pairs but also in ensembles of coupled dynamics. Therefore, our work shows that these approaches are suitable for a reliable detection of interactions between real-world signals.

Future studies of this work could include the extension of the measure L in order to infer connectivity from networks of dynamics. Moreover, it would be interesting to study directional couplings from the mean fields of multiple ensembles of dynamics. Aspects that can be studied are the effect of the topology of the dynamics and the role of perturbations. The perturbations include but are no limited to the presence of noise, removal of connections and changes of the inherent dynamics.

Bibliography

[1] G. Alba, E. Pereda, S. Mañas, L. D Méndez, M.R. Duque, A. González, and J. J. González. The variability of eeg functional connectivity of young adhd subjects in different resting states. *Clinical neurophysiology*, 127(2):13211330, 2016.

[2] R. G. Andrzejak. *Epilepsy, The intersection of Neurosciences, Biology, Mathematics, Engineering and Physics.:125*. Osorio et.al edition, 2011.

[3] R. G. Andrzejak, D. Chicharro, K. Lehnertz, and F. Mormann. Using bivariate signal analysis to characterize the epileptic focus: The benefit of surrogates. *Phys. Rev. E*, 83:046203, 2011.

[4] R. G. Andrzejak, A. Kraskov, H. Stögbauer, F. Mormann, and T. Kreuz. Bivariate surrogate techniques: Necessity, strengths, and caveats. *Phys. Rev. E*, 68:066202, 2003.

[5] R. G. Andrzejak, K. Lehnertz, F. Mormann, C. Rieke, P. David, and C. E. Elger. Indications of nonlinear deterministic and finite-dimensional structures in time series of brain electrical activity: Dependence on recording region and brain state. *Phys. Rev. E*, 64:061907, 2001.

[6] R. G. Andrzejak, K. Schindler, and C. Rummel. Nonrandomness, nonlinear dependence, and nonstationarity of electroencephalographic recordings from epilepsy patients. *Phys. Rev. E*, 86:046206, 2012.

[7] R.G. Andrzejak, G. Widman, K. Lehnertz, C. Rieke, P. David, and C.E. Elger. The epileptic process as nonlinear deterministic dynamics in a stochastic environment: an evaluation on mesial temporal lobe epilepsy. *Epilepsy Research*, 44(2):129 – 140, 2001.

[8] J. Arnhold, P. Grassberger, K. Lehnertz, and C. E. Elger. A robust method for detecting interdependencies: application to intracranially recorded eeg. *Physica D*, 134:419–430, 1999.

[9] A. Attanasio and U. Triacca. Detecting human influence on climate using neural networks based granger causality. *Theoretical and Applied Climatology*, 103(1-2):103–107, 2011.

[10] A. Pikovsky B. Kralemann, M. Rosenblum. *Damoco2, http://www.stat.physik.uni-potsdam.de/ mros/damoco2.html*, 2014.

[11] B. Bezruchko, V. Ponomarenko, M. G. Rosenblum, and A. S. Pikovsky. Characterizing direction of coupling from experimental observations. *Chaos*, 13(1):179–184, 2003.

[12] R. P. Brent. *Algorithms for Minimization Without Derivatives*. Prentice-Hall, Englewood Cliffs, 1973.

[13] G. Buzsaki. *Rhythms of the Brain*. Oxford University Press, 1 edition, 2006.

[14] D. Chicharro and R. G. Andrzejak. *http://ntsa.upf.edu/downloads/*, 2009.

[15] D. Chicharro and R. G. Andrzejak. Reliable detection of directional couplings using rank statistics. *Phys. Rev. E*, 80:026217, 2009.

[16] L. Cimponeriu, M.G. Rosenblum, T. Fieseler, J. Dammers, M. Schiek, M. Majtanik, P. Morosan, A. Bezerianos, and P. A. Tass. Inferring asymmetric relations between interacting neuronal oscillators. *Progress of Theoretical Physics Supplement*, 150:22 – 36, 2003.

[17] P. T. Clemson and A. Stefanovska. Discerning non-autonomous dynamics. *Physics Reports*, 542(4):297 – 368, 2014.

[18] Sebastian E., A. Pikovsky, and M. Rosenblum. From complete to modulated synchrony in networks of identical hindmarsh-rose neurons. *European physical journal special topics*, 222(10):2407 – 2416, 2013.

[19] L. Faes, G. Nollo, and A. Porta. Information-based detection of nonlinear granger causality in multivariate processes via a nonuniform embedding technique. *Phys. Rev. E*, 83:051112, 2011.

[20] L. Faes, G. Nollo, and A. Porta. Information domain approach to the investigation of cardio-vascular, cardio-pulmonary, and vasculopulmonary causal couplings. *Frontiers in Physiology*, 2:80, 2011.

[21] M. D. Fox, A. Z. Snyder, J. L. Vicent, M. Corbetta, D. C. Van Essen, and M. E. Raichle. The human brain is intrinsically organized into dynamc, anticorrelated functional networks. *PNAS*, 102:9673–9678, 2005.

[22] D. Gabor. Theory of communication. *J. IEEE*, 93(26):429–457, 1946.

[23] C. Hiemstra and J. D. Jones. Testing for linear and nonlinear granger causality in the stock price-volume relation. *The Journal of Finance*, 49(5):1639–1664, 1994.

[24] A. Čenys, G. Lasiene, and K. Pyragas. Estimation of interrelation between chaotic observables. *Physica D: Nonlinear Phenomena*, 52(2):332 – 337, 1991.

[25] E. R. Kandel, J. H. Schwartz, and T. M. Jessell. *Principles of Neural Science*. McGraw-Hill Medical, 4th edition, July 2000.

[26] H. Kantz and T. Schreiber. *Nonlinear time series analysis*, volume 7 of *Cambridge Nonlinear Science Series*. Cambridge University Press, Cambridge, 1997.

[27] B. Kralemann, L. Cimponeriu, M. Rosenblum, A. Pikovsky, and R.. Mrowka. Uncovering interaction of coupled oscillators from data. *Phys. Rev. E*, 76:055201, 2007.

[28] B. Kralemann, L. Cimponeriu, M. Rosenblum, A. Pikovsky, and R. Mrowka. Phase dynamics of coupled oscillators reconstructed from data. *Phys. Rev. E*, 77:066205, 2008.

[29] B. Kralemann, M. Frühwirth, A. Pikovsky, M. Rosenblum, T Kenner, J Schaefer, and M Moser. In vivo cardiac phase response curve elucidates human respiratory heart rate variability. *Nat. Commun.*, 4:2418, 2013.

[30] B. Kralemann, A. Pikovsky, and M. Rosenblum. Reconstructing phase dynamics of oscillator networks. *Chaos*, 21(2), 2011.

[31] B. Kralemann, A. Pikovsky, and M. Rosenblum. Reconstructing effective phase connectivity of oscillator networks from observations. *New Journal of Physics*, 16(8):085013, 2014.

[32] D. Kugiumtzis. Direct-coupling information measure from nonuniform embedding. *Phys. Rev. E*, 87:062918, 2013.

[33] P. Laiou and R. G. Andrzejak. Coupling strength versus coupling impact in nonidentical bidirectionally coupled dynamics. *Phys. Rev. E*, 95:012210, 2017.

[34] Z. Levnajić. Derivative-variable correlation reveals the structure of dynamical networks. *The European Physical Journal B*, 86(7), 2013.

[35] Z. Levnajić and A. Pikovsky. Untangling complex dynamical systems via derivative-variable correlations. *Scientific Reports*, 4:5030, 2014.

[36] E. N. Lorenz. Deterministic Nonperiodic Flow. *J. Atmos. Sci.*, 20(2):130–141, 1963.

[37] I. I. Mokhov and D. A. Smirnov. El niosouthern oscillation drives north atlantic oscillation as revealed with nonlinear techniques from climatic indices. *Geophysical Research Letters*, 33(3):L03708, 2006.

[38] A. Montalto, S. Stramaglia, L. Faes, G. Tessitore, R. Prevete, and D. Marinazzo. Neural networks with non-uniform embedding and explicit validation phase to assess granger causality. *Neural Networks*, 71:159 – 171, 2015.

[39] H. Moon and T. C. Lu. Network catastrophe: Self-organized patterns reveal both the instability and the structure of complex networks. *Scientific Reports*, 5:9450, 2015.

[40] R. Mrowka, L. Cimponeriu, A. Patzak, and M. G. Rosenblum. Directionality of coupling of physiological subsystems: age-related changes of cardiorespiratory interaction during different sleep stages in babies. *American Journal of Physiology - Regulatory, Integrative and Comparative Physiology*, 285(6):R1395–R1401, 2003.

[41] K. Nallakumar. The synchronously flashing aggregative fireflies of peninsular malaysia. *Biodiversity*, 4:11–16, 2003.

[42] M. Paluš. Multiscale atmospheric dynamics: Cross-frequency phase-amplitude coupling in the air temperature. *Phys. Rev. Lett.*, 112:078702, 2014.

[43] M. Paluš and A. Stefanovska. Direction of coupling from phases of interacting oscillators: An information-theoretic approach. *Phys. Rev. E*, 67:055201, 2003.

[44] M. Paluš and M. Vejmelka. Directionality of coupling from bivariate time series: How to avoid false causalities and missed connections. *Phys. Rev. E*, 75:056211, 2007.

[45] P. Papiotis. *A computational approach to studying interdependence in string quartet performance*. PhD thesis, Universitat Pompeu Fabra, September 2015.

[46] A. Pikovsky and M. Rosenblum. Self-organized partially synchronous dynamics in populations of nonlinearly coupled oscillators. *Physica D: Nonlinear Phenomena*, 238(1):27 – 37, 2009.

[47] A. Pikovsky and M. Rosenblum. Dynamics of globally coupled oscillators: Progress and perspectives. *Chaos: An Interdisciplinary Journal of Nonlinear Science*, 25(9):097616, 2015.

[48] A. Pikovsky, M. Rosenblum, and J. Kurths. *Synchronization : a universal concept in nonlinear sciences*. The Cambridge nonlinear science series. Cambridge University Press, Cambridge, 2001.

[49] A. S. Pikovsky, M. G. Rosenblum, and J. Kurths. Synchronization in a population of globally coupled chaotic oscillators. *EPL (Europhysics Letters)*, 34(3):165, 1996.

[50] R. Q. Quiroga, J. Arnhold, and P. Grassberger. Learning driver-response relationships from synchronization patterns. *Phys. Rev. E*, 61:5142–5148, 2000.

[51] R. Q. Quiroga, T. Kreuz, and P. Grassberger. Event synchronization: A simple and fast method to measure synchronicity and time delay patterns. *Phys. Rev. E*, 66:041904, 2002.

[52] M. Rosenblum, L. Cimponeriu, and A. Pikovsky. *Coupled Oscillators Approach in Analysis of Bivariate Data*, pages 159–180. Wiley-VCH Verlag GmbH and Co. KGaA, 2006.

[53] M. G. Rosenblum, L. Cimponeriu, A. Bezerianos, A. Patzak, and R. Mrowka. Identification of coupling direction: Application to cardiorespiratory interaction. *Phys. Rev. E*, 65:041909, 2002.

[54] M. G. Rosenblum and A. S. Pikovsky. Detecting direction of coupling in interacting oscillators. *Phys. Rev. E*, 64:045202, 2001.

[55] C. Rummel, E. Abela, M. Müller, M. Hauf, O. Scheidegger, R. Wiest, and K. Schindler. Uniform approach to linear and nonlinear interrelation patterns in multivariate time series. *Phys. Rev. E*, 83:066215, 2011.

[56] C. Rummel, M. Müller, G. Baier, F. Amor, and K. Schindler. Analyzing spatio-temporal patterns of genuine cross-correlations. *Journal of Neuroscience Methods*, 191:94 – 100, 2010.

[57] Tomislav S., Valentina T., P. V. E. McClintock, and A. Stefanovska. Coupling functions in networks of oscillators. *New Journal of Physics*, 17(3):035002, 2015.

[58] B. Schelter, M. Winterhalder, R. Dahlhaus, J. Kurths, and J. Timmer. Partial phase synchronization for multivariate synchronizing systems. *Phys. Rev. Lett.*, 96:208103, 2006.

[59] S. J. Schiff, P. So, T. Chang, R. E. Burke, and T. Sauer. Detecting dynamical interdependence and generalized synchrony through mutual prediction in a neural ensemble. *Phys. Rev. E*, 54:6708–6724, 1996.

[60] T. Schreiber. Measuring information transfer. *Phys. Rev. Lett.*, 85:461–464, 2000.

[61] T. Schreiber and A. Schmitz. Surrogate time series. *Physica D: Nonlinear Phenomena*, 142(3):346 – 382, 2000.

[62] J. P. Shaffer. Multiple hypothesis testing. *Annual Review of Psychology*, 46:561–584, 1995.

[63] L. W. Sheppard, A. C. Hale, S. Petkoski, P. V. E. McClintock, and A. Stefanovska. Characterizing an ensemble of interacting oscillators: The mean-field variability index. *Phys. Rev. E*, 87:012905, 2013.

[64] V. N. Smelyanskiy, D. G. Luchinsky, A. Stefanovska, and P. V. E. McClintock. Inference of a nonlinear stochastic model of the cardiorespiratory interaction. *Phys. Rev. Lett.*, 94:098101, 2005.

[65] D. A. Smirnov and R. G. Andrzejak. Detection of weak directional coupling: Phase-dynamics approach versus state-space approach. *Phys. Rev. E*, 71:036207, 2005.

[66] D. A. Smirnov and B. P. Bezruchko. Estimation of interaction strength and direction from short and noisy time series. *Phys. Rev. E*, 68:046209, 2003.

[67] T. Stankovski, A. Duggento, P. V. E. McClintock, and A. Stefanovska. Inference of time-evolving coupled dynamical systems in the presence of noise. *Phys. Rev. Lett.*, 109:024101, 2012.

[68] T. Stankovski, P. V. E. McClintock, and A. Stefanovska. Coupling functions enable secure communications. *Phys. Rev. X*, 4:011026, 2014.

[69] S. H. Strogatz. *Nonlinear dynamics and chaos: with applications to physics, biology, chemistry, and engineering*. Studies in nonlinearity. Westview Press, Cambridge (Mass.), 1994.

[70] R. Suresh, D. V. Senthilkumar, M. Lakshmanan, and J. Kurths. Transition to complete synchronization and global intermittent synchronization in an array of time-delay systems. *Phys. Rev. E*, 86:016212, 2012.

[71] F. Takens. Detecting strange attractors in turbulence. In David Rand and Lai-Sang Young, editors, *Dynamical Systems and Turbulence, Warwick 1980*, volume 898 of *Lecture Notes in Mathematics*, pages 366–381. Springer Berlin Heidelberg, 1981.

[72] C. Tenreiro. Fourier series-based direct plug-in bandwidth selectors for kernel density estimation. *Journal of Nonparametric Statistics*, 23:533–545, 2011.

[73] J. Theiler. Spurious dimension from correlation algorithms applied to limited time-series data. *Phys. Rev. A*, 34:2427–2432, 1986.

[74] I. Vlachos and D. Kugiumtzis. Nonuniform state-space reconstruction and coupling detection. *Phys. Rev. E*, 82:016207, 2010.